Shape For Contact

Alberto Rodriguez Garcia

CMU-RI-TR-13-21

Submitted in partial fulfillment of the
requirements for the degree of
Doctor of Philosophy in Robotics

The Robotics Institute
Carnegie Mellon University
Pittsburgh, Pennsylvania 15213

August 2013

Thesis Committee:
Matthew T. Mason, Chair
Siddhartha Srinivasa
Howie Choset
Vijay Kumar, *University of Pennsylvania*

To Nuria and Zoe,

Because it is only when work becomes a small part of life
that you can work without fear.

Shape For Contact

Alberto Rodriguez

PhD Thesis
Robotics Institute - Carnegie Mellon University
August 23, 2013

Abstract

Given a desired function for an effector, what is its appropriate shape? This thesis addresses the problem of designing the shape of a rigid end effector to perform a given manipulation task. It presents three main contributions: First, it describes the contact kinematics of an effector as the product of both its shape and its motion, and assumes a fixed motion model to explore the role of shape in satisfying a certain manipulation task. Second, it formulates that manipulation task as a set of constraints on the geometry of contact between the effector and the world. Third, it develops tools to transform those contact constraints into an effector shape for general 1-DOF planar mechanisms and general 1-DOF spatial mechanisms, and discusses the generalization to mechanisms with more than one degree of freedom.

We describe the case studies of designing grippers with invariant grasp geometry, grippers with improved grasp stability, and grippers with extended grasp versatility. We further showcase the techniques with the design of the fingers of the MLab hand, a three-fingered gripper actuated with a single motor, capable of exerting any combination of geometrically correct enveloping or fingertip grasps of spherical, cylindrical, and prismatic objects of varying size.

Contents

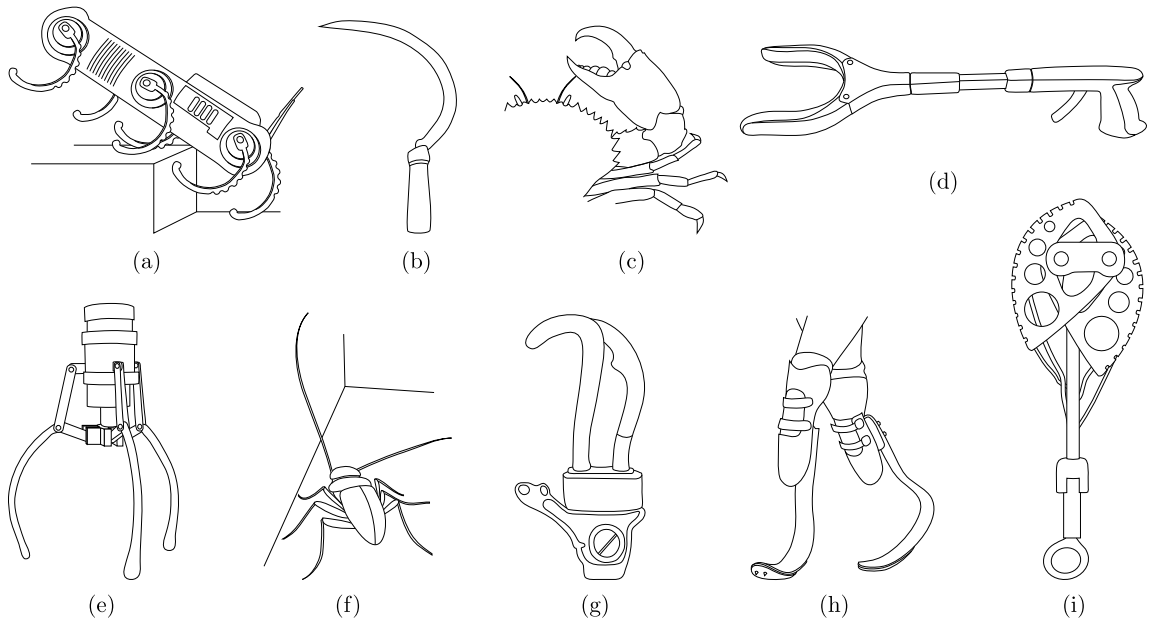

Figure 1: Effectors whose shape is relevant to their mechanical function: (a) hexapod robot "RHex", (b) sickle, (c) crab pincer, (d) manual gripper "Grip'n Grab", (e) claw crane, (f) cockroach antennae, (g) prosthetic hook, (h) prosthetic leg, and (i) rock-climbing cam.

1 Introduction

"... that form ever follows function. This is the law."
— Louis Sullivan, *The Tall Office Building Artistically Considered.*

Robotic hands, and end effectors in general, play a privileged role in the manipulation chain. They contact the world. That role gives them an advantageous position to convey function and contribute to a solution to the manipulation problem, either by means of their actions or by means of their design. In this thesis we look at effector shape as a design freedom and explore its possible role in expressing effector function.

The connection between effector function and effector shape is ubiquitous in manipulation and all of robotics (Figure 1). Although most of the applications developed in this thesis are in the context of robotic hands, the intended scope is larger. We will make use of the term *end effector*, or simply *effector*, to refer to a hand or one of its fingers, or a foot, or a tool, or in general any surface meant to contact the world.

Effector shape plays an important role in determining the reaction of an object to contact and has the potential to express mechanical intelligence, yet the design of effector shape has been relatively neglected compared to other areas of manipulator design research. Particularly significant is the prolonged interest in transforming actuation into carefully planned motion by using mechanical devices such as cams, linkages, or gears. In this thesis, instead, we assume a fixed *motion* or actuation for a mechanism and study the role of *shape* in producing mechanical intelligence. We start motivating the relevance of shape to manipulation by describing the mechanics of rock-climbing cams, a simple but functional device that served as inspiration for this thesis.

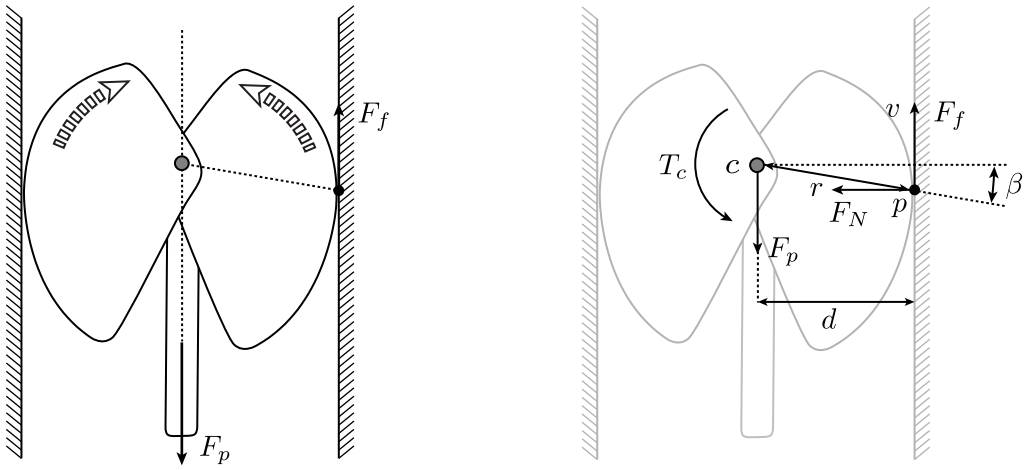

(a) (b)

Figure 2: (a) Spring loaded cam for rock-climbing. The device uses the wedge effect to transform pulling force F_p into magnified friction force F_f. (b) Static force diagram of contact mechanics between cam and wall, for a given wall width $2d$.

1.1 Example: Rock-Climbing Cam

A spring loaded rock-climbing cam, Figure 1i, is a device used to secure anchor points in cracks in the rock face. As illustrated in Figure 2a, the device uses the mechanical advantage of the wedge effect to convert pulling force F_p into magnified friction force F_f.

The condition for static equilibrium—zero torque at the rotation center c—applied to the force diagram in Figure 2b yields a relation between the friction force, the coefficient of friction of the wall μ, and the contact angle β:

$$\begin{aligned} & r \cdot F_f \cos\beta = r \cdot F_N \sin\beta \\ [F_f \leq \mu F_N] \qquad & F_N \tan\beta \leq \mu F_N \\ & \beta \leq \tan^{-1}\mu \end{aligned} \tag{1}$$

which illustrates that the contact angle β is a particularly relevant factor to the design of rock-climbing cams. Leaving aside the details of how to chose the optimal β (which in practice has a strong experimental component) for this discussion it is enough to note that planning for a specific value of β is critical in the design of rock-climbing cams.

For a known wall width $2d$, it is rather straightforward to impose a given contact angle β. The shape of the cam can adapted to follow the desired tangent v at the desired contact point p. That condition, however, is only for a specific wall width d, and cracks in the rock face are not of a fixed width.

To avoid carrying a large collection of cams—one for each crack size—the question arises of whether it is possible for a single cam to satisfy that contact pattern for different wall widths, that is, if it is possible for the contact pattern to be invariant with the size of the crack, and preserve the contact angle β while the cam opens and closes adapting to different wall widths.

The short answer is yes. Each wall width in Figure 3 imposes a different tangential contraint on the shape of the cam. The key observation that leads to this thesis is that those tangential

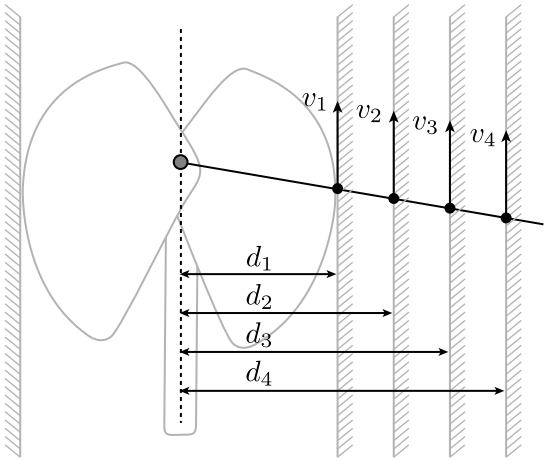

Figure 3: Invariant loading pattern for different wall widths. The cam must satisfy the tangents v_i for different wall widths d_i.

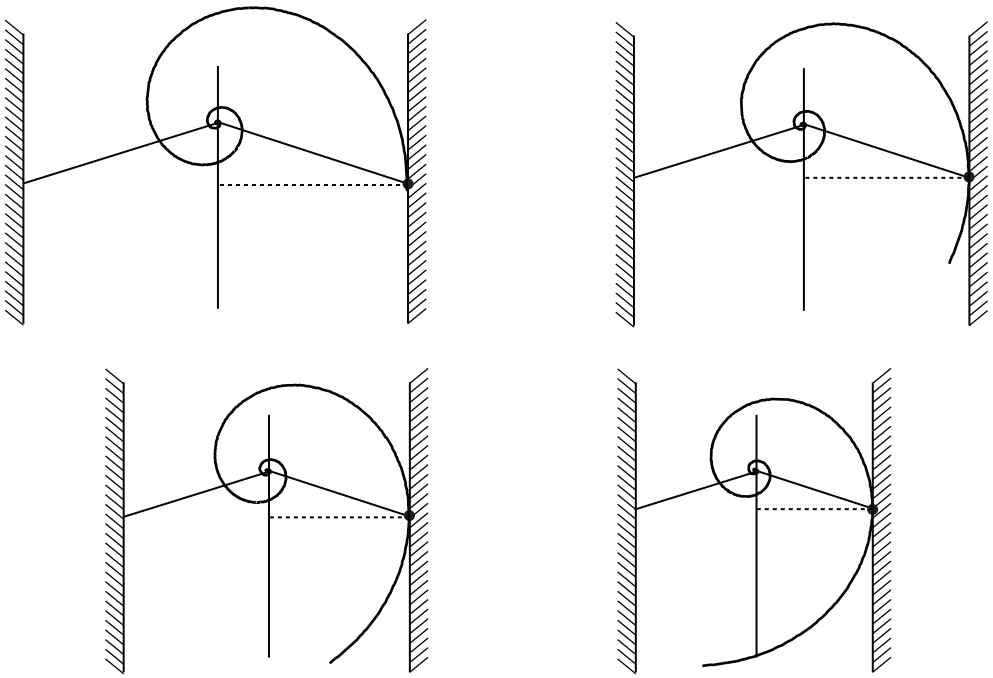

Figure 4: A cam following a logarithmic spiral yields invariant contact geometry with respect to the width of the crack.

constraints can be integrated to obtain the shape of the cam. In this thesis we show how to formulate and solve the problem in a more general setting. We will see in Section 6.1.1 that, for the specific case of the rock-climbing cam, the solution is a logarithmic spiral (Figure 4).

It is interesting to notice that logarithmic spirals have been used for decades in the design of climbing cams. The invention of the modern rock-climbing cam is attributed to Raymond Jardine [31], who used a logarithmic spiral, with camming angle $\beta = 13.5°$.

The climbing cam is an inspirational exercise of making use of shape at the service of simplicity and robustness. There is no required sensing or control involved in its operation. The details to achieve a functional contact geometry with the wall are worked out by the "mechanical intelligence" of its design. The main question we explore in this thesis is how to formalize that principle and apply it to other domains.

1.2 Shape and Simple Hands

This thesis also grew out of our interest in simple hands, focused on enveloping grasps of objects with uncertain pose and shape [40, 62, 63, 41, 49, 50].

The traditional approach to grasping uses knowledge of object geometry and grasp mechanics to plan for contact points. We refer to that approach as "putting the fingers in the right place", illustrated in Figure 5a. In this context, the details of phalange shape are of little consequence, since usually only the tip of the finger is involved in the grasp. The adaptation to variations in object shape and pose is achieved through active control of several actuators per finger.

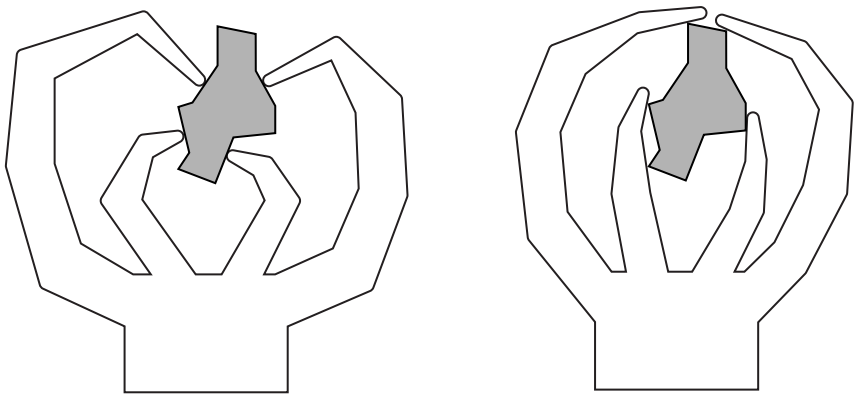

(a) "Putting the fingers in the right place" (b) "Letting the fingers fall where they may"

Figure 5: Two different approaches to grasping: (a) The hand uses knowledge of object geometry and grasp mechanics to plan for contact points. (b) The hand closes with the expectation that the details of hand/object interaction will be worked out automatically.

Simple hands, often with one actuator per finger, or even one actuator driving several fingers, lack the necessary complexity to realize planned contact formations. For hands like the prosthetic hook in Figure 1g, the crab pincer in Figure 1c, or the manual gripper in Figure 1d, the job of gracefully adapting to shape and pose variations may fall on mechanical attributes other than kinematic complexity, such as compliance or underactuation, or, as explored in this thesis, on finger shape.

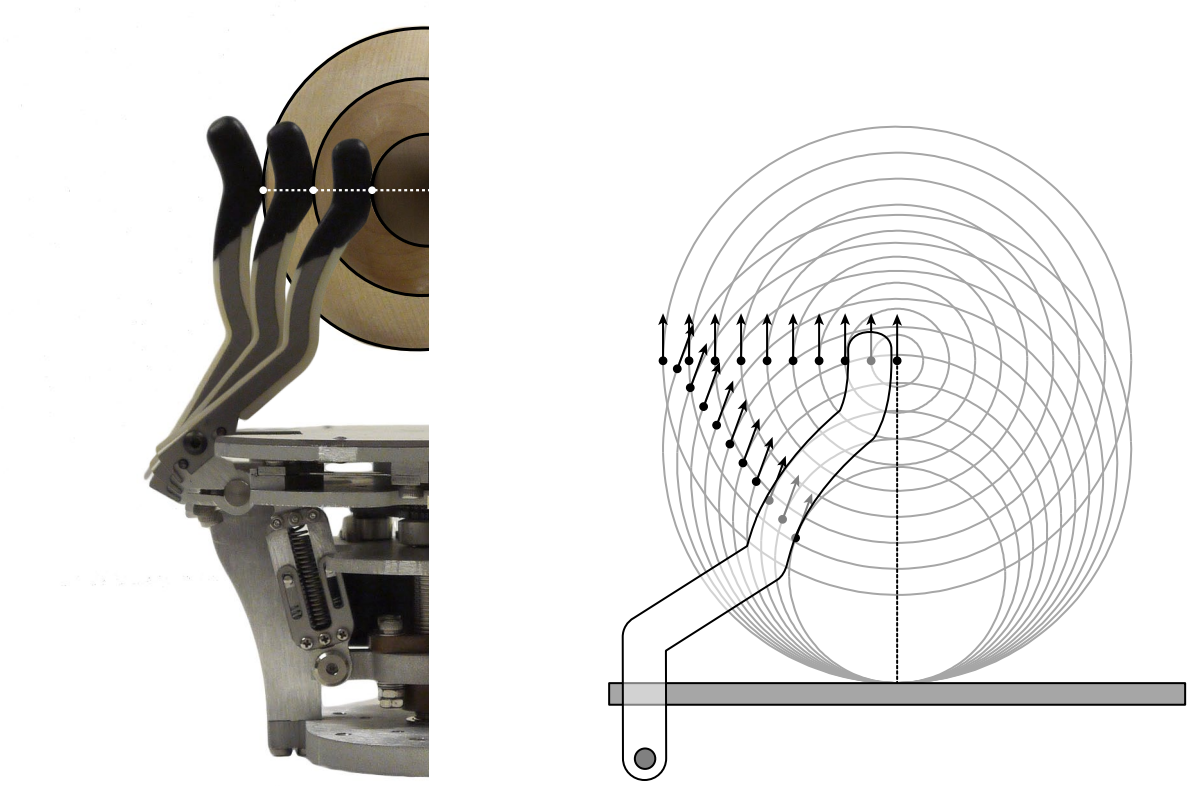

(a) (b)

Figure 6: (a) MLab Hand grasping spheres of varying size with invariant contact geometry. (b) Set of contacts used to design the fingers. They enable the MLab Hand to grasp spheres of varying size both in enveloping and fingertip configuration.

Simple hands adapt to varying shapes and poses by the emergent interaction of hand with object. We can refer to this approach by "letting the fingers fall where they may", illustrated in Figure 5b. Hollerback [30] describes it as "the details work themselves out as the hand and object interact rather than being planned in advance". In this context, the actual forms of the phalanges and the palm become important.

If it is the case that phalange form is important, what principles should guide its design? It depends on context—the specific application, the hand design philosophy, and in particular on the function assigned to the fingers. In this thesis we explore possible roles of fingers in producing "mechanical intelligence", including adaptation to variations in object shape and pose (Section 6.2), improvement of the stability of a grasp (Section 7.2), and extension of the versatility of a gripper (Section 8.2). Figure 6 shows a motivating example of how the fingers of grippers can be designed for a purpose. Their curved phalanges yield geometrically correct fingertip and enveloping grasps of spheres of varying size. We will approach the problem in greater detail in Section 8.2 with the design of the fingers of the MLab Hand.

1.3 Shape and Mechanical Function

The goal of this thesis is to develop techniques to synthesize shape for the purpose of some manipulation task, or mechanical function. The starting point of the thesis is that manipulation task, which we will assume is described as set of constraints to the geometry of contact between the effector and the rest of the world.

In practice, we will specify a set of contacts in the workspace that the effector should reproduce when driven by its actuator, and develop techniques to integrate those contacts into an effector shape.

The basic idea of using contacts to represent a mechanical function is illustrated in Figure 7, with the task of pushing a disk along a given path. In an idealized frictionless quasistatic world, an effector should contact the disk with a contact normal along the path tangent as in Figure 7b. In the presence of friction or perturbations, the disk would surely deviate from the desired path. In that case, the "corrective" contacts shown in Figure 7c are chosen to stabilize its motion. Examining these additional corrective contact constraints would allow one to reject a point pusher, or a flat pusher, and instead choose a cupped shape.

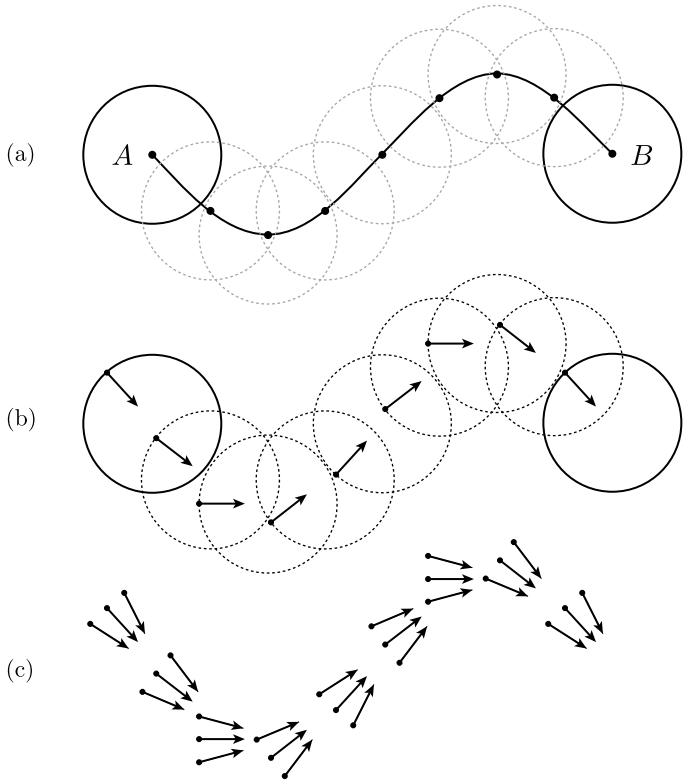

Figure 7: An example task represented by a set of contact constraints. (a) The goal is to move the disk from A to B along the given path. (b) For the disk to follow the path, the effector must push it along the path tangent, which gives a continuum of contact constraints. (c) We can add extra "corrective" constraints to make the push robust to perturbations, such as friction.

Reducing a desired function to contact constraints is quite common in manipulation, for example is used to characterize the rigidity of a grasp, or to explain the stability of an object at rest on a table. The power of the representation lies within the assumption that once the task is described as a set of geometric contact conditions, we can forget about the task itself, and the rest of the world. We just need to design a mechanism or a control algorithm capable of contacting as specified.

1.4 Contributions

The main contribution of this thesis is to formalize the shape synthesis problem as one of satisfying a pattern of contacts. In particular:

- We describe an effector as the product of its shape and its motion (Section 3). First, we represent the effector motion, independently of the shape attached to it, by a vector field in $\mathcal{W} \times T$, cartesian product space of the workspace and the mechanism configuration space. Then, assuming a fixed motion model, we explore the role of shape in satisfying a certain mechanical purpose.
- We assume the desired mechanical purpose is represented by a set of constraints on the geometry of contact between the effector and the rest of the world, and formulate conditions for the effector to satisfy them (Section 4).
- We then use the formalizations of shape, motion, and contact constraint to formulate the shape synthesis problem (Section 5).

In the second part of this thesis we particularize the formulation to planar rotational joints (Section 6), general 1-DOF planar actuation (Section 7), and general 1-DOF spatial actuation (Section 8). We use those case studies to describe approaches and issues in solving the shape synthesis problem, and to illustrate three principles to guide the design of finger form: grasp invariance with respect to variations in object shape and/or pose, improvement of grasp stability, and extending grasp versatility. We finish in Section 9 discussing limitations of the proposed formulation, possible extensions to the multi-DOF case, and other future directions.

2 Related Work

There is a long history of using mechanical design in place of online computation, especially in that period before computers were available. The principle of replacing computation with mechanical design has been called "mechanical intelligence" (Ulrich [74]), "hard automation" (Canny and Goldberg [13]) "morphological computation" (Pfeifer and Iida [53]) or "adaptive mechanics" (Gosselin [25]), as further developed in Figure 8.

Mechanisms such as cams, linkages, or gears have been used for centuries to synthesize motion (Hartenberg and Denavit [28], Paul [51], Shigley and Uicker [68], McCarthy [42]) or to compute (Svoboda [69]). One notable application is the design of kinematic and passive-dynamic mechanisms to produce walking machines (Raibert [54], McGeer [43], Collins et al. [15], Gomes and Ruina [24]), which dates back at least to the 18th century, with a walking device based on Chebyshev's linkage to transform rotational motion into approximate straight-line motion (Lucas [38]). In an example particularly pertinent to the present work, McGeer [43] examines foot shape and the resulting evolution of contact between foot and ground.

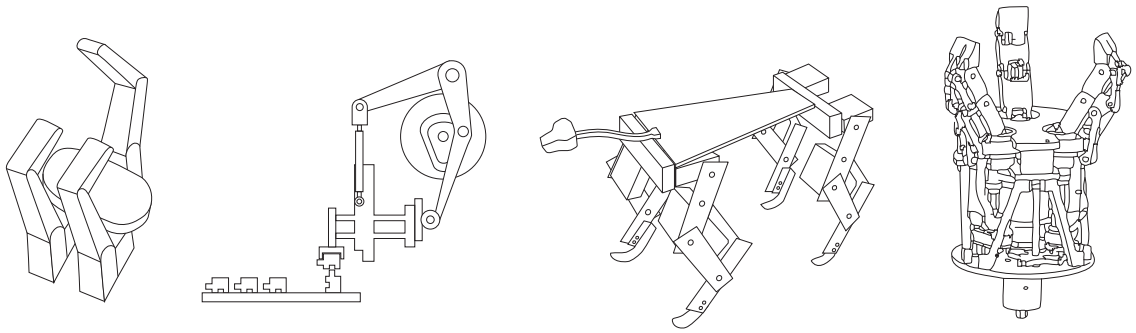

(a) (b) (c) (d)

Figure 8: Different instantiations of the principle to replace online computation by mechanical design: (a) Mechanical intelligence of the UPenn Hand (precursor to the Barrett Hand [1]). Ulrich [74] designs a three fingered robotic hand with reduced kinematic complexity. Each finger has two degrees of freedom, but is driven by a single motor. When in contact, a clutch mechanism disengages the proximal phalange to facilitate enveloping grasps. (b) Canny and Goldberg [13] illustrate the concept of hard automation with an example of an assembly plan "compiled" into a mechanism (figure adapted from [23]). (c) Morphological computation of Puppy, a robotic quadruped developed by Pfeifer and Iida [53] that locomotes with no sensory feedback (figure adapted from [53]). (d) Adaptive mechanics of the Sarah Hand [35] (precursor to the RobotIQ gripper [58]). Rubinger et al. [64] design an underactuated robotic hand that passively adapts to the shape and size of an object.

Perhaps most relevant to this thesis is the desire to build simple yet capable robotic hands, where compliance and underactuation take care of shape adaptation which in turn reduces the need for complex mechanics and controls (Hirose and Umetani [29], Ulrich et al. [75, 74], Rubinger et al. [64], Laliberte and Gosselin [35], Dollar and Howe [18, 20], Birglen et al. [5], Mason et al. [62, 41], Odhner et al. [47], Ciocarlie et al. [14]).

In this thesis, rather than *actuation* or *compliance*, we target the *shape* of a mechanism as conveyor of mechanical intelligence. In general, shape alone is not enough to solve a manipulation problem, however, it is a "cheap" design freedom with potential benefits both in terms of simplicity and robustness. The circular leg design by Moore et al. [45] for the robotic hexapod Rhex (Saranli et al. [66]) is a clear example of shape, in combination with compliance, servicing simplicity. Robustness is also a potential benefit of shape design, as illustrated in Section 1.1 with the design of rock climbing-cams shaped to provide sufficient grip over a wide range of crack widths.

In the contexts of grasping and robotic hands, shape has rarely played an important role. The most common approach is to rely on grasp planners to choose fixed contact points based on precise knowledge of object shape and pose. Even when sliding or rolling contacts are modeled, they are seldom exploited to design functional phalanx shape.

Dollar and Howe [19] reviewed the designs of 20 compliant and underactuated robotic hands, all of which used cylindrical or flat straight fingers and with no cited principle to guide the designs of their shapes. Theobald et al. [70] is one of the first exceptions, with a gripper with curved fingers designed to enable autonomous rock acquisition. More recently, Kragten et al. [34] considered curving the contact area of distal phalanges to improve the stability of

precision grasps. Lynch et al. [39] studied the roles of hand shape and motion in dynamic manipulation.

Automation, and in particular applications like part feeding and assembly, raised interest in shape synthesis. Traps, fences and chamfers are examples of mechanical features where physical interaction and the reaction to contact can be planned in advance and hard-coded in the design of the mechanism. Redford and Boothroyd [55], Boothroyd et al. [7], and [56] are pioneering works in systematically approaching the problems of part feeding and part orienting. Boothroyd and Dewhurst [6] presents a comprehensive collection of early mechanical feeding and orienting techniques.

Berretty et al. [3] analyzed the interaction between objects and traps to automate the design of vibratory bowl feeders. With a similar goal Berretty et al. [2], Peshkin and Sanderson [52] and Wiegley et al. [77] worked on the design of fences to reorient parts moving in a conveyor belt. Brokowski et al. [9] proposed adding curved tails to the end of those fences, and showed that their shape was key to control the resulting uncertainty in the pose of the reoriented part. The technique they used to design the tails of fences resembles the approach to shape design in this thesis. Still in the context of part feeding, Zhang and Goldberg [78] systematized the design of the phalanges of a parallel jaw gripper to passively align parts in the vertical plane, and Whitney et al. [76] designed curved chamfers to simplify the assembly of rigid parts.

The goal of producing general purpose motion with cams and gears also lead to the study of shape. Reuleaux [57] introduced in the 19th century the concept of kinematic pair as an attempt to abstract motion constraints between contacting bodies. For ideal joints such as prismatic or revolute (lower pairs), shape is of little consequence. But for pairs where contact is maintained between curved surfaces like in the case of cams or gears (higher pairs), shape plays a key role. Several works in the early 90s approached the problem of qualitative shape understanding for kinematic pairs (Joskowicz [32], Joskowicz and Addanki [33], Faltings [21], Forbus et al. [22]), with the goal of modeling the effect that small alterations to the shape of the contacting bodies had to their respective configuration spaces (Lozano-Perez [36]). Gupta and Jakiela [26] designed kinematic pairs by sweeping a fixed shape along a predefined path and numerically "carving" the other shape. Inspired by applications such as vibratory bowl feeders and part mating, Caine [11, 12] studied the design of shape from motion constraints.

In Caine's work, as in most previous work described in this section, shape synthesis is understood as the inverse of the motion planning problem[1]. A desired mechanical interaction between two bodies is specified by voiding regions on their relative configuration spaces. Shape synthesis is approached then as an effort to invert those constraints imposed on the motion of an object. In contrast, this thesis represents mechanical function as a collection of geometric contact constraints. Rather than constraining the relative free motions between two bodies, we specify where and how they should contact each other.

Using contact rather than motion constraints has important implications. It is more difficult to represent dynamic tasks, since contacts are localized and static constraints, but the problem becomes more tractable, specially in 3D. Contacts constraints are represented by vectors, while motion contraints are regions of the configuration space, which are higher dimensional and more complex to represent.

Contact kinematics, the study of how the contact location between two objects changes with their motions, is then key for this thesis, in particular to understand how they affect

[1]Noted by Lozano-Perez [37].

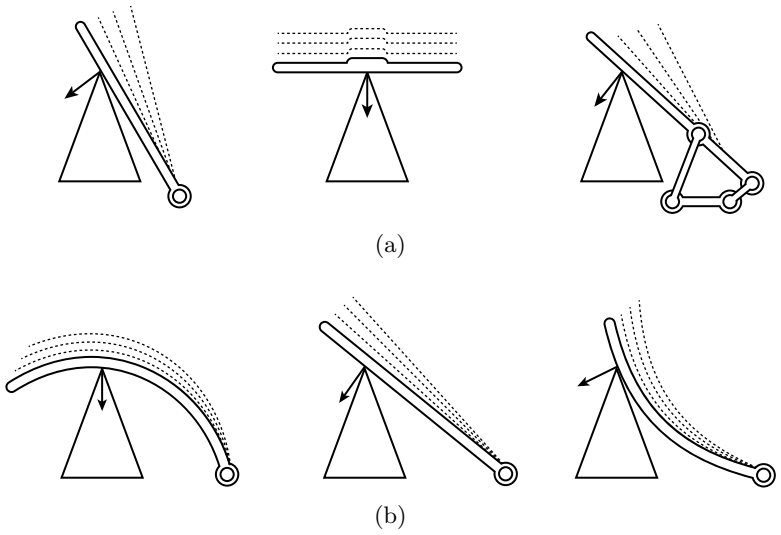

Figure 9: (a) Three actuation mechanisms and (b) three effector shapes contacting an object at a given point. The expected reaction of the object to that contact varies both with the motion and the shape of the effector.

mechanical function. Cai and Roth [10] studied the motion of the contact point between two objects that roll-slide on each other and Montana [44] provided a more formal approach to the same problem. We will assume all that as a given here, and focus on the synthesis problem.

3 End Effectors: Shape and Motion

The kinematic behavior of an end effector is determined, in part, by its motion and its shape. As illustrated in Figure 9, both shape and motion have an impact in that kinematic function. In this section we formalize the model of an effector, and introduce the concepts of motion field, motion orbit, and orbit space.

The respective contributions of shape and motion to the function of an effector are intertwined. The suitability of a shape depends on motion, and vice versa. In this thesis we assume a fixed given effector motion and address the shape synthesis problem.

We make two simplifying assumptions on the effector:

- The effector is rigid. There is no compliance on the shape of the effector nor on the actuation mechanism.
- The effector actuation is via a 1-DOF smooth mechanism in a planar or spatial workspace.

We make no assumptions on the object, other that it is possible to describe the desired task as a set of contacts. We formally define now the concept of effector:

Let $\mathcal{W} = \mathbb{R}^d$ be the workspace of the effector, with $d = 2$ (planar mechanisms) or $d = 3$ (spatial mechanisms). The effector is driven by a 1-DOF mechanism, whose space of configurations $T = [t_{\min}, t_{\max}]$ is parametrized by t the *motion parameter*. Without loss of generality, we assume that $0 \in T$.

The shape of the effector is a smooth manifold of dimension $(d-1)$ rigidly attached to the driving mechanism, i.e., a smooth curve for the planar case or a smooth surface for the

spatial case. Let $s \in S = [s_{\min}, s_{\max}]$ or $(u, v) \in U \times V = [u_{\min}, u_{\max}] \times [v_{\min}, v_{\max}]$ be the *shape parameters* mapping the effector shape for the planar and spatial cases. For simplicity of notation, and unless noted otherwise, we will use $s \in S$ to refer indistinctively both to the planar and spatial cases. We define then:

Definition 1 (Effector)**.** An effector E is a smooth map from shape and motion parameters to workspace points $E : S \times T \mapsto \mathcal{W}$, where for a fixed t, $E(\cdot, t)$ parametrizes with unit speed a rigid transformation of the curve or surface $E(s, 0)$.

E describes the motion (parametrized by t) of a rigid manifold (parametrized by s) as actuated by the mechanism, so that $E(s, t_0)$ maps S to the effector shape in $\mathcal{W}$ at configuration t_0. For simplicity, we will refer by shape to the curve or surface $E(s, 0)$.

3.1 Motion Field

The *motion field* is a representation of the motion imposed by a mechanism. Given an effector $E(s, t)$ whose shape lies at p at configuration t_0, i.e., $p \in E(S, t_0)$, we define the velocity v_p imposed by the mechanism to the effector particle lying at p by differentiating $E(s, t)$ with respect to the motion parameter t and holding the shape parameter s fixed. The construction is illustrated in Figure 10. Note that v_p is independent of the shape of the effector (we differentiate with respect to t), and that it can be defined for any $p \in \mathcal{W}$ and any $t \in T$, since we can always come up with a shape that attached to the effector crosses p for configuration t.

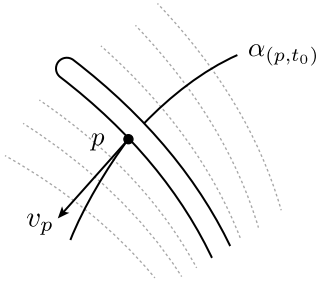

Figure 10: Given a point p in the workspace and a configuration of a mechanism t_0, we define the motion field $\mathcal{M}$ at (p, t_0) as the tangent to the trajectory $\alpha_{(p,t_0)}$ that a particle would follow if attached to any effector passing through p at configuration t_0 driven by that same mechanism.

For reasons that will become apparent later, it is important to consider the velocity v_p imposed by the effector at p in the extended space $\mathcal{W} \times T$, cartesian product of the workspace and the mechanism configuration space. We define then:

Definition 2 (Motion Field)**.** Motion field $\mathcal{M}$ of a mechanism at a workspace point $p \in \mathcal{W}$ and configuration t is the vector field representing the direction of imposed effector motion:

$$\begin{array}{rccl} \mathcal{M}: & \mathcal{W} \times T & \rightarrow & \mathcal{T}(\mathcal{W} \times T) \\ & (p, t) & \mapsto & (v_p, 1) = \left(\frac{\partial E(s,t)}{\partial t}, 1\right) \end{array}$$

where E is an effector such that $E(s, t) = p$, and where $\mathcal{T}(\mathcal{W} \times T)$ is the tangent bundle of $\mathcal{W} \times T$.

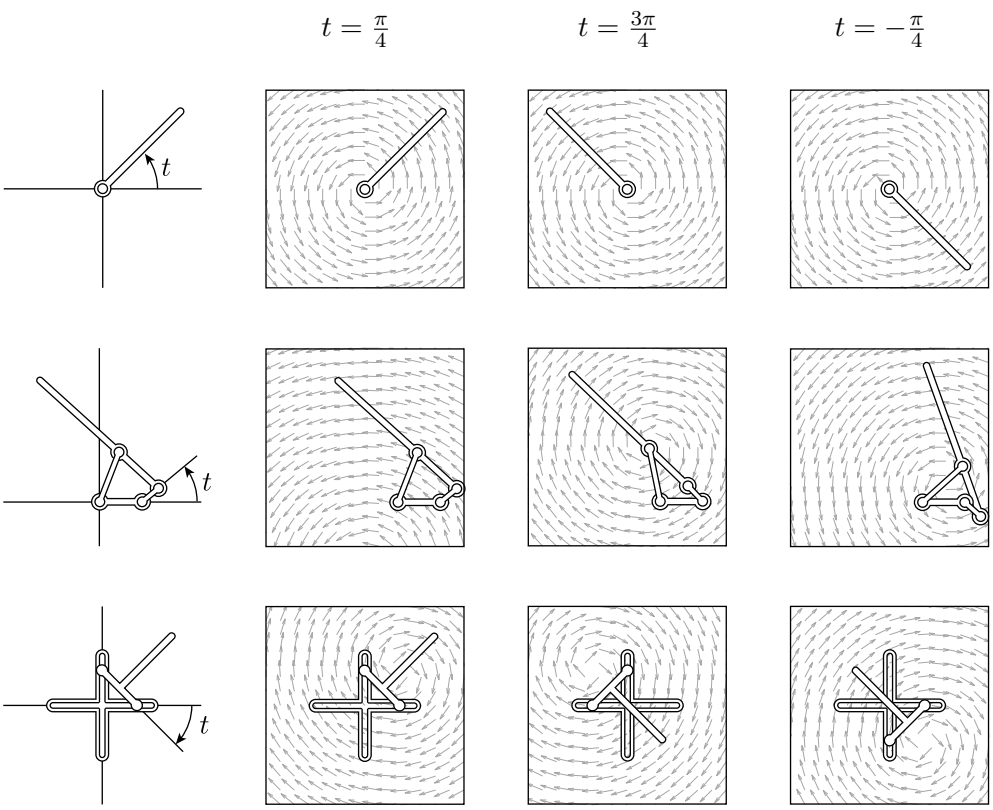

Figure 11: Motion field for three mechanisms: (top) rotational joint, (middle) Hoekens linkage, and (bottom) elliptic trammel. Columns are slices $t = \frac{\pi}{4}$, $t = \frac{3\pi}{4}$, and $t = -\frac{\pi}{4}$ of the motion field. Note that slices $t = \text{const}$ are the motion field of a rotational joint. The location of the rotation center of that joint is known as the instantaneous center of rotation. Note also that the motion field of a revolute joint is invariant with t.

Note that the last component of $\mathcal{M}(p, t)$ is always 1. This reflects the fact that the effector is continuously actuated by a 1-DOF mechanism. Figure 11 shows the motion fields of three different planar actuation mechanisms: a rotational joint, a Hoekens linkage, and an elliptic trammel. There is no conceptual difference between the motion fields of planar and spatial mechanisms, except that they live on spaces of different dimension. In Section 8 we will see examples of motion fields for spatial mechanisms.

In the following subsections we see that the motion field $\mathcal{M}$ partitions the space $\mathcal{W} \times T$ into disjoint motion orbits. Those motion orbits will constitute the domain of influence of contact constraints.

3.2 Motion Orbits

In differential geometry, the flow Φ of a smooth vector field V on a manifold $\mathcal{N}$ is defined, for every point $q \in \mathcal{N}$, as the trajectory that a particle at q would describe following an integral

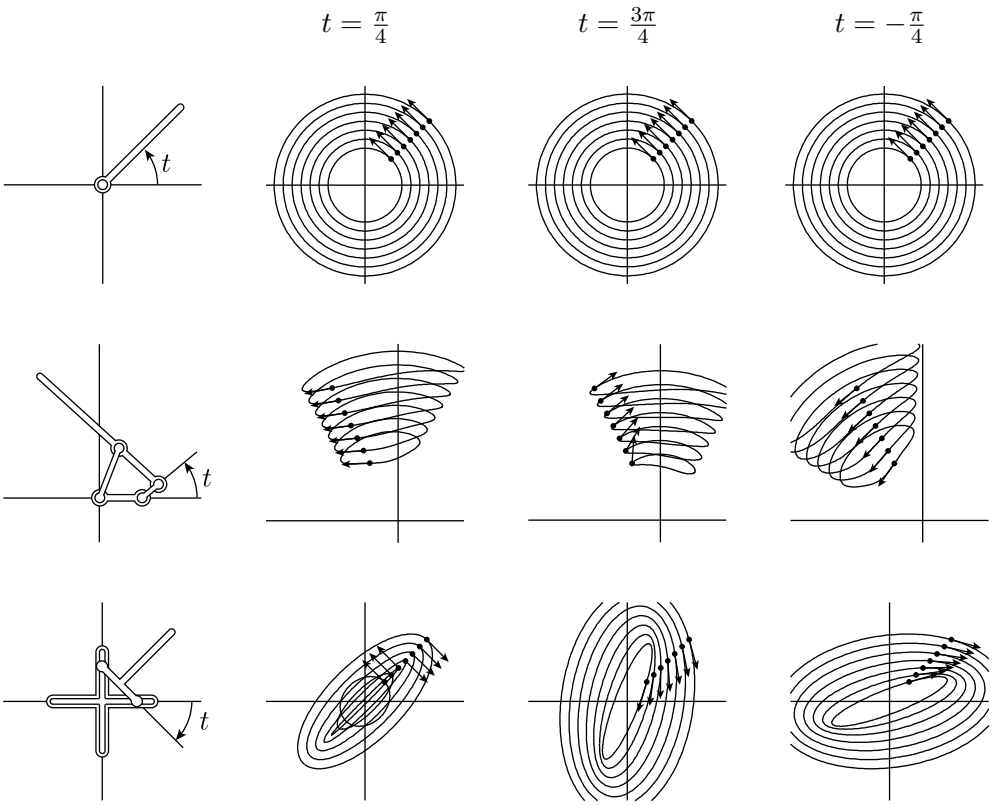

Figure 12: Motion orbits for three mechanisms: (top) rotational joint, (middle) Hoekens linkage, and (bottom) elliptic trammel. The figure shows the projection of the motion orbits to the workspace $\mathcal{W}$ for three different initial mechanism configurations: $t = \frac{\pi}{4}$, $t = \frac{3\pi}{4}$ and $t = -\frac{\pi}{4}$. Note that the motion orbits of a rotational joint are invariant with t.

curve of V. Let $\Phi_{\mathcal{M}}$ be the flow of the motion field $\mathcal{M}$:

$$\begin{array}{rccc} \Phi_{\mathcal{M}}: & (\mathcal{W} \times T) \times \mathbb{R} & \rightarrow & \mathcal{W} \times T \\ & ((p,t),u) & \mapsto & \Phi_{\mathcal{M}}((p,t),u) \end{array} \tag{2}$$

where $\Phi_{\mathcal{M}}((p,t),\cdot)$ is the unique integral curve of $\mathcal{M}$ passing through (p,t). Intuitively, the motion flow $\Phi_{\mathcal{M}}$ describes the trajectory in $\mathcal{W} \times T$ followed by an effector particle positioned at p when the mechanism starts at configuration t. We define the associated *motion orbit* as:

Definition 3 (Motion Orbit)**.** The motion orbit of a point $(p,t) \in \mathcal{W} \times T$, under the motion flow $\Phi_{\mathcal{M}}$, is the set $\Phi_{(p,t)} = \{\Phi_{\mathcal{M}}((p,t),u) : u \in \mathbb{R}\}$.

Note that, for the case of 1-DOF effectors, the projections of the motion orbits from $\mathcal{W} \times T$ to the workspace $\mathcal{W}$ are also known as the coupler curves of the mechanism [28]. Figure 12 shows those projections for three initial values of the motion parameter t and three different mechanisms: a rotational joint, a Hoekens linkage, and an elliptic trammel. Again, there is no conceptual difference between the motion orbits of planar and spatial mechanisms. In Section 8 we will see an example for a spatial mechanism.

3.3 Space of Orbits

In this section we study the structure of the set of motion orbits, which will later be used in Section 4 to formalize contact constraints. Recall now that motion orbits are the integral curves of the motion field $\mathcal{M}$, and that they are defined for all $(p, t) \in \mathcal{W} \times T$.

It is always the case for a smooth non-vanishing vector field that its integral curves define a 1-dimensional foliation of the space. Intuitively, a foliation is a decomposition of the space into "parallel" subspaces of smaller dimension, like decomposing a plane into parallel lines, or 3D space into parallel planes. In particular, a 1-dimensional foliation is a decomposition of the space into non-intersecting curves.

In our case, $\mathcal{M}$ is a never-vanishing smooth vector field, since the last component is constant equal to 1 and the mechanism is smooth by assumption. Hence, the set of motion orbits decomposes the space $\mathcal{W} \times T$ into the union of non-intersecting curves. This allows us to define an equivalence relationship $\sim$, where two points in $\mathcal{W} \times T$ are equivalent, if and only if they share the same motion orbit:

$$(p, t_1) \sim (q, t_2) \quad \iff \quad \Phi_{(p,t_1)} = \Phi_{(q,t_2)} \tag{3}$$

The space of orbits is then defined as:

Definition 4 (Orbit Space)**.** The orbit space is the quotient space $\mathcal{O} = (\mathcal{W} \times T)/_{\sim}$ where each element in $\mathcal{O}$ is representative of all points equivalent to each other.

For the purpose of visualization, we chose a single point from each class to represent it. When chosen properly, those representative points form a lower dimensional subspace or section in $\mathcal{W} \times T$ easy to visualize. Sections that are transversal to the motion flow $\Phi_{\mathcal{M}}$ and are crossed once and only once by each motion orbit are specially appropriate.

An example is the set $\{t = t_0\}$ through which all orbits are guaranteed to cross once and only once, since they are strictly monotonic in t. The section $\{t = 0\}$ is a natural choice, given that in Section 3 we refer by effector shape to the curve $E(\cdot, 0)$, using $t = 0$ as the reference mechanism configuration. Note also that the section $\{t = 0\}$, i.e. the set $\mathcal{W} \times \{0\}$, is pointwise equivalent to $\mathcal{W}$. Hence we can think of the effector shape as a curve or surface both in the workspace $\mathcal{W}$ or in the orbit space $\mathcal{O}$.

The characterization of shape and motion in this section leads us in Section 4 to the argument that the domain of influence of contact constraints are entire motion orbits. This will allow us to transport contact constraints to a single mechanism configuration (the orbit space) and overcome the difficulty posed by not knowing a priori for what configuration of the effector should a contact constraint be satisfied.

4 Contact Constraints

In this section we formalize contact constraints and define operations on them. For simplicity of exposition we will only refer here to first order contact constraints, that is, we will match the tangents of object and effector. In Section 9.2 we discuss how in a very similar fashion, when required by the task, we can also impose higher order contact constraints, for example to the curvature of the effector. Optionally, as illustrated in Figure 7c, we can also approximate higher order constraints by combining first order ones.

We will represent contact constraints indistinctively by their contact normals η or their corresponding tangent spaces ω. A representation in terms of contact normals will be more apt to formulate the problem because they give a common notation for the 2D and 3D cases. Tangent vectors and tangent planes, however, will be more readily used to describe applications and implementations.

We begin with the definition of two types of constraints. Given a point p in the workspace and a desired contact normal η:

Definition 5 (Contact Constraint)**.** A contact constraint $(p, \eta) \in \mathbb{R}^2 \times S^1$ (or in $\mathbb{R}^3 \times S^2$ for spatial constraints) is satisfied by an effector $E(s,t)$ if there are $t_0 \in T$ and $s_0 \in S$ (or $(u_0, v_0) \in S$ for spatial constraints) such that:

$$E(s_0, t_0) = p \quad \text{and} \quad \eta \cdot \left. \frac{\partial E(s, t_0)}{\partial s} \right|_{s=s_0} = 0$$

or

$$E(u_0, v_0, t_0) = p \quad \text{and} \quad \begin{cases} \eta \cdot \left. \frac{\partial E(u, v_0, t_0)}{\partial u} \right|_{u=u_0} = 0 \\ \eta \cdot \left. \frac{\partial E(u_0, v, t_0)}{\partial v} \right|_{v=v_0} = 0 \end{cases}$$

Definition 6 (Shape Constraint)**.** A shape constraint $((p, t_0), \eta) \in (\mathbb{R}^2 \times T) \times S^1$ (or in $(\mathbb{R}^3 \times T) \times S^2$ for spatial constraints) is satisfied by an effector $E(s,t)$ if at configuration t_0 there is $s_0 \in S$ (or $(u_0, v_0) \in S$ for spatial constraints) such that:

$$E(s_0, t_0) = p \quad \text{and} \quad \eta \cdot \left. \frac{\partial E(s, t_0)}{\partial s} \right|_{s=s_0} = 0$$

or

$$E(u_0, v_0, t_0) = p \quad \text{and} \quad \begin{cases} \eta \cdot \left. \frac{\partial E(u, v_0, t_0)}{\partial u} \right|_{u=u_0} = 0 \\ \eta \cdot \left. \frac{\partial E(u_0, v, t_0)}{\partial v} \right|_{v=v_0} = 0 \end{cases}$$

A *contact constraint* is satisfied if there is any configuration of the effector that is consistent with the desired normal. A *shape constraint* specifies a particular configuration of the effector. Thus there is a very simple relation between contact and shape constraints: A contact constraint (p, η) is satisfied if and only if at least one of the shape constraints in the set $\{((p,t), \eta) : t \in T\}$ is satisfied.

4.1 Constraint Propagation

As mentioned earlier, the main challenge in enforcing contact constraints is not knowing for what configuration of the effector each constraint should be satisfied. It is easier, however, to enforce shape constraints. They include a specific effector configuration. Then, to enforce a contact constraint (p, η) we will look at it as the whole set of shape constraints it represents, and follow the recipe:

1. Transform the set of shape constraints $\{((p,t), \eta) : t \in T\}$ so they all apply to the same effector configuration, $t = 0$; and
2. make sure one of them is satisfied.

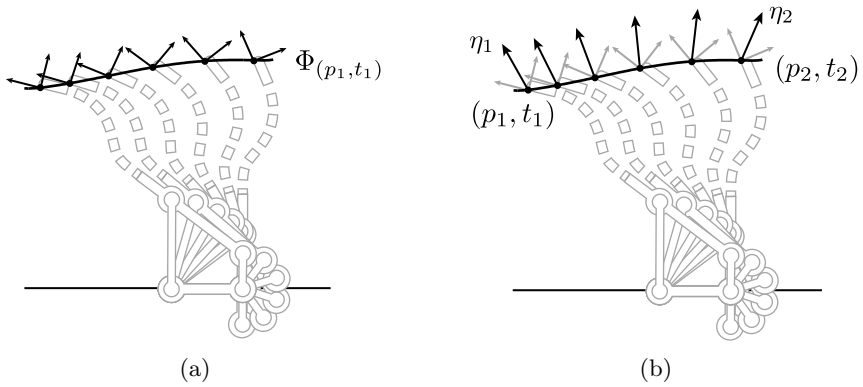

Figure 13: (a) Moving frame for a Hoekens linkage between configurations $t_1 = \frac{\pi}{2}$ and $t_2 = -\frac{\pi}{2}$. The moving frame changes as if rigidly attached to the mechanism. (b) The propagation of the tangential constraint η_1 at point (p_1, t_1) to η_2 at point (p_2, t_2) is so that the constraint is held invariant in the moving frame ($\eta_2 = P_{(p_1,t_1)\to(p_2,t_2)}(\eta_1)$).

To transform a shape constraint is to find an equivalent shape constraint for a different mechanism configuration. To formalize the idea we first derive an expression for equivalent constraints. We will use the terms *moving frame* and *fixed frame* to refer to coordinate frames rigidly attached respectively to the effector and to the workspace, as in Figure 13a.

Consider two equivalent points $(p_1, t_1) \sim (p_2, t_2)$ in the extended space $\mathcal{W} \times T$ of an effector (defined in Section 3.3). By definition, equivalent points share the same orbit, and therefore the same effector particle crosses both p_1 at configuration t_1, and p_2 at t_2. The normals η_1 and η_2 of the effector at those two points must be identical in the moving frame, since the effector, by assumption is rigid. We will say that the constraints $((p_1, t_1), \eta_1)$ and $((p_2, t_2), \eta_2)$ are equivalent, that is an effector satisfies one iff it satisfies the other.

By *constraint propagation* we mean the process that transforms constraint $((p_1, t_1), \eta_1)$ into the equivalent constraint $((p_2, t_2), \eta_2)$, which, by construction, is defined between any pair of equivalent points (Figure 13b). We note by $P_{(p_1,t_1)\to(p_2,t_2)}(\cdot)$ the function that maps normal η_1 to normal η_2. In general we will propagate all shape constraints to configuration $t = 0$.

An important consequence of constraint propagation is that an effector satisfies a shape constraint $((p, t), \eta)$ if and only if it satisfies any of the shape constraints propagated within the same orbit:

$$((p,t),\eta) \;\Leftrightarrow\; \left\{((q,t'), P_{(p,t)\to(q,t')}(\eta))\right\}_{(q,t')\in\Phi_{(p,t)}} \tag{4}$$

Then, we say the domain of influence of a shape constraint is the entire motion orbit it represents. We can only impose one constraint per motion orbit.

4.2 Constraint Locus

In this section we find a representation of contact constraints in orbit space independent of the configuration of the mechanism. By definition, a contact constraint (p, η) is satisfied if and only if one of the shape constraints $\{((p, t), \eta) : t \in T\}$ is satisfied. Following (4), each shape constraint is satisfied if and only if its propagation to $t = 0$ is satisfied. Consequently, a

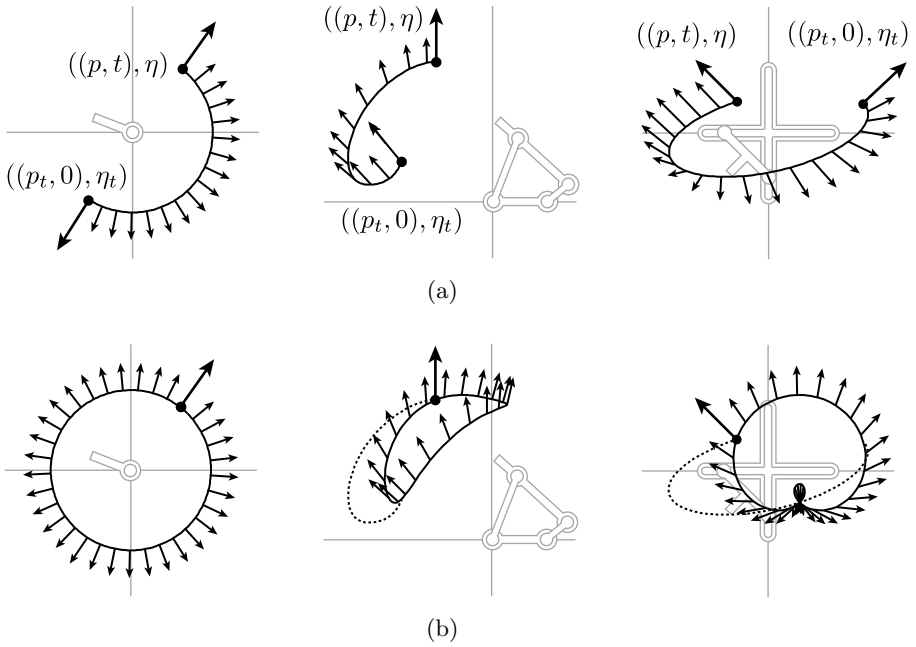

Figure 14: Example constraint locus for three contact constraints and three mechanisms: (left) rotational joint, (center) Hoekens linkage, and (right) elliptic trammel. (a) The shape constraint $((p,t),\eta)$ is propagated to $((p_t,0),\eta_t)$ at slice $t=0$ through a motion orbit. (b) The constraint locus is generated by repeating the process for all possible values of t.

contact constraint is fully represented in orbit space $\mathcal{O}$ by a set of propagated constraints. We call that set of propagated constraints, the *constraint locus*:

Definition 7 (Constraint Locus)**.** Let (p,η) be a contact constraint, $\eta_t = P_{(p,t)\to(p_t,0)}(\eta)$ the propagation of $((p,t),\eta)$ to $t=0$ through the motion orbit $\Phi_{(p,t)}$, and $(p_t,0)$ the corresponding point in $\mathcal{W}\times T$ where the constraint gets propagated. The constraint locus of (p,η) is the set $\mathcal{L}_{(p,\eta)} = \{((p_t,0),\eta_t) : t \in T\}$

Intuitively, we can think of the constraint locus as the pre-image of the constraint by the mechanism, i.e., the set of points in the workspace that, if they were to belong to the shape of the effector for $t=0$, they would eventually cross p as the mechanism advances.

The constraint locus represents the contact constraint for all possible mechanism configurations. From a practical point of view, to satisfy a contact constraint, we need to construct its locus and choose an effector shape that, attached to the mechanism for $t=0$, crosses the locus consistently with the propagated constraints. Figure 14 shows examples of constraint locus of three different contact constraints and three mechanisms.

Note that, as illustrated in Figure 14, the locus of a constraint does not follow the natural evolution of a mechanism motion orbit. The following proposition relates the shapes of locus and orbits:

Proposition 1 (Orbit vs. Locus)**.** *The locus of a contact constraint in orbit space is equal to the orbit of the constraint induced by the inverted mechanism*[2]*.*

[2]The inverse of a mechanism is obtained by exchanging moving and fixed reference frames.

Proof. Let $A : T \longrightarrow \mathbb{SE}(2)$ be the mechanism map for the effector. We represent $A(t)$ as an homogenous matrix so that point $(p, 0)$ is mapped to $(A(t) \cdot p, t)$. The orbit associated with a constraint is the set $\Phi = \{(A(t) \cdot p, t) : t \in T\}$ and its locus $\mathcal{L} = \{(q, t_q) : A(t_q) \cdot q = p\}$. Then, for every point $q \in \mathcal{L}$, we have:

$$A(t_q) \cdot q = p \;\Leftrightarrow\; q = A^{-1}(t_q) \cdot p$$

that is, q is in the locus induced by A if and only if q is in the orbit induced by A^{-1}, the inverted mechanism. □

5 Shape Synthesis: Formulation

We have now all the machinery in place to formulate the shape synthesis problem. We first recall the key concepts:

- An *effector* is a map $E(s, t) : \mathcal{S} \times T \mapsto \mathcal{W}$ describing the motion (parametrized by t) of a rigid curve (parametrized by s) or surface (parametrized by (u, v)) driven by a mechanism.
- The *shape* of the effector is the curve $E(s, 0)$, describing the contact surface of the effector for configuration $t = 0$ of the mechanism.
- The *motion* of the effector is captured by a vector field $\mathcal{M}(p, t)$ in $\mathcal{W} \times T$ that determines the direction of motion to follow by a particle at p rigidly attached to the mechanism for configuration t.
- *Motion orbits* are the integral curves of $\mathcal{M}$, the trajectories followed by particles of the effector as actuated by the mechanism. Assuming smoothness of the mechanism, motion orbits never intersect each other in the extended space $\mathcal{W} \times T$.
- The *orbit space* $\mathcal{O}$ of the effector is a one-to-one representation of the set of motion orbits. Our choice of orbit space is the slice $t = 0$ of $\mathcal{W} \times T$. The shape of the effector can be described as a curve or surface α in $\mathcal{O}$.
- A *shape constraint* $((p, t), \eta)$ is an imposition on the effector to locally comply with η at location p and configuration t. It propagates along motion orbits while being held invariant in the moving frame. It is satisfied iff its propagation to $\mathcal{O}$ is satisfied, and it is represented in $\mathcal{O}$ as a point.
- A *contact constraint* (p, η) is an imposition on the effector to locally comply with ω at location p of the workspace for an unspecified configuration of the mechanism. It is satisfied iff any of the shape constraints in $\{((p, t), \eta)\}_{t \in T}$ are satisfied, and it is represented in $\mathcal{O}$ as a locus of constraints $\mathcal{L}_{(p,\eta)}$.
- An effector $E(s, t)$ locally satisfies a constraint (p, η) if and only if its shape, described as a curve or surface in $\mathcal{O}$, crosses the locus $L_{(p,\eta)}$ consistent with the constraint.

The shape synthesis problem formulates as:

Problem 1 (Shape for Contact)**.** *Let $\mathcal{M}$ be the motion field of an effector, $\{(p_i, \eta_i)\}_{i=1\ldots N}$ a set of contact constraints, and $\mathcal{L}_{(p_i,\eta_i)}$ the corresponding loci in $\mathcal{O}$. Find a curve (for planar effectors) or surface (for spatial effectors) α in $\mathcal{O}$ that crosses all loci consistently.*

Note that loci described by different contact constraints may intersect each other. The points of the orbit space $\mathcal{O}$ where they intersect will likely induce inconsistent constraints if α crosses them. To find a complete solution, we must find a shape that is consistent with all loci, and without any inconsistencies. If there are no inconsistent constraints, by construction the effector induced by the shape α locally satisfies all constraints.

The approach to propagate constraints allows us to express them in the reference pose of the effector at $t = 0$, even without knowing at which pose t each constraint will be enforced. The key is the use of the extended space $\mathcal{W} \times T$.

6 Case Study: Planar Rotational Joints

Rotational joints are one of the most widely used driving mechanisms. They are analyzed in depth by Rodriguez and Mason [59, 60]. They are also a particularly simple and illustrative example for the shape synthesis problem.

What makes rotational joints particularly simple? First, by construction, the instantaneous center of rotation of a rotational joint is constant, and as a consequence, its motion field and motion orbits are invariant with respect to the configuration of the mechanism. See Figure 11 and Figure 12 for examples. Second, we will see that for rotational joints, orbits and locus follow the same path. These will simplify the problem enough to allow us to find analytic solutions and give guarantees of existence of those solutions.

We mentioned in Section 4.1 that one of the main challenges to impose a contact constraint is that we do not know a priori what configuration of the mechanism the effector should satisfy it. However, since in this case motion orbits are invariant with the mechanism configuration, so will be the conditions for constraint satisfaction. To better illustrate it consider the following example problem (Figure 15):

> *Scale-invariant contact problem:* Given an object shape in the plane, p a point in the boundary of the object, and c the location of the finger's revolute joint, find the finger shape that makes contact at p despite the scaling of the object.

A solution to the scale-invariant contact problem would yield a finger shape that preserves the contact location as well as the contact normal with the scale of the object. As a consequence, and most importantly, many properties governing the mechanics of the interaction between effector and object would also be preserved. To solve it, we apply the two-step procedure induced in Section 5: First we construct the loci of the set of contact constraints; and second we find a curve consistent with it. Both steps become simpler in the case of rotational joints.

The locus of a contact constraint is constructed by propagating the constraint to all possible mechanism configurations along corresponding motion orbits. Note that, in the case of a rotational joint, motion orbits are concentric circles invariant to the configuration of the mechanism. We construct the loci by repeating the process to all constraints.

Proposition 1 in Section 4.2 shows that the locus of a constraint induced by a mechanism follows a motion orbit of the inverted mechanism. Given that the inverted mechanism of a rotational joint is the same rotational joint operating in reverse, locus and orbit follows the same

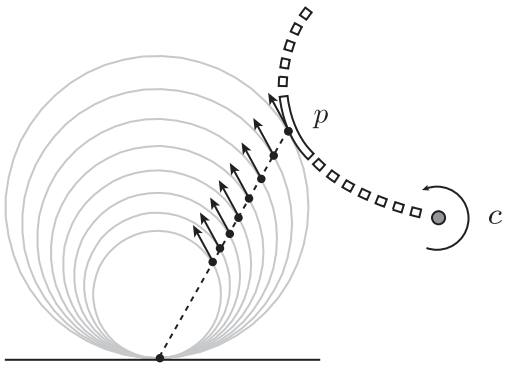

Figure 15: The scale-invariant contact problem: What finger shape actuated by a rotational joint from c contacts the disk at p and yields invariant contact geometry with respect to the scale of a disk?

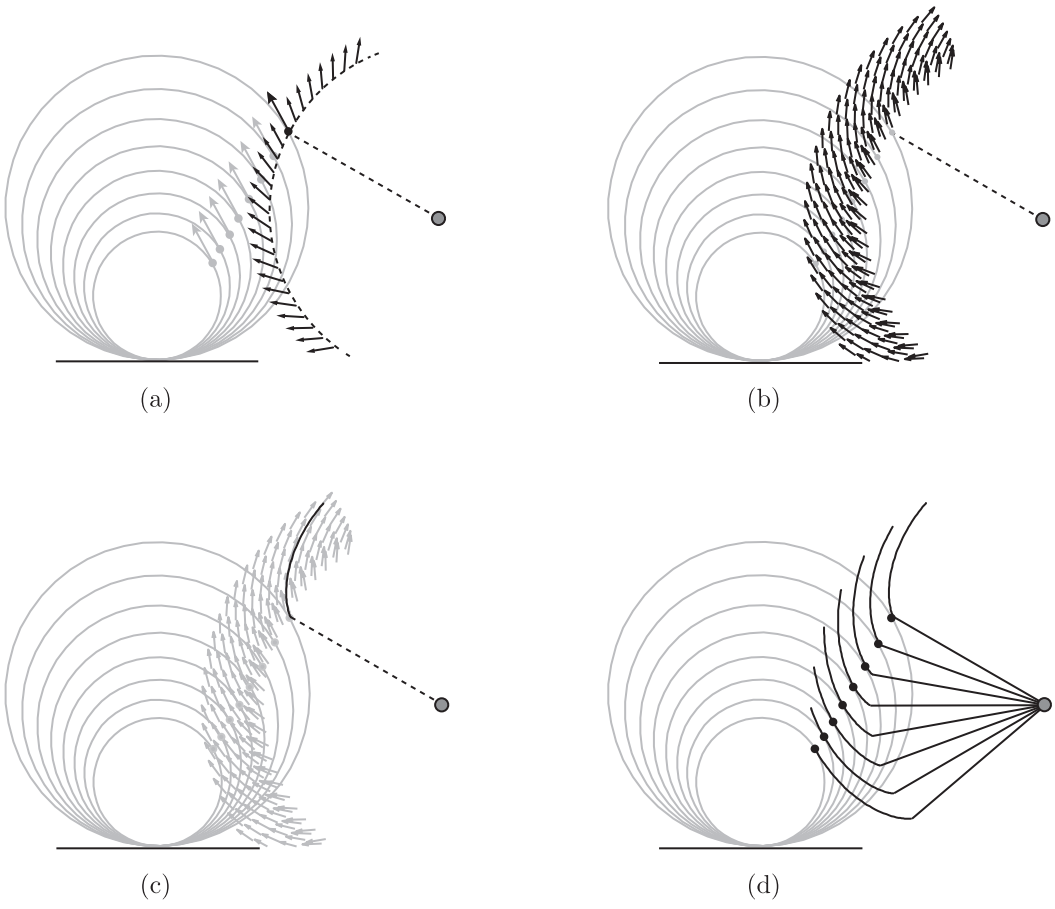

Figure 16: (a) The locus of one contact constraint propagated by a rotational joint is equivalent to the parallel transport of that constraint along a circular arc. (b) Loci of the set of imposed contraints in the scale-invariant contact problem. It produces a smooth vector field $\mathcal{F}$. (c) Integral curve of the resultant vector field. (d) By construction, the integral curve is a solution to the scale-invariant contact problem.

trajectory. In practice, to construct the locus of a constraint we will do the parallel transport of the constraint along a circular orbit while preserving the angle between the constraint vector and the orbit, as illustrated in Figure 16a. In Figure 16b the process is applied to all contacts to generate the loci.

In this section we pay special attention to the case where the set of imposed constraints forms a 1-dimensional continuous set. We call *contact curve* $\mathcal{C}$ to the trace of the base location of the constraints in that set, for example to the segment connecting p to the base of the disks in Figure 15. We are interested in characterizing under what conditions that 1-dimensional set of contraints uniquely determine the solution to the shape synthesis problem.

Let $r(\cdot) : \mathcal{C} \mapsto \mathbb{R}^+$ be the function that maps points along the contact curve to their corresponding distance to the center of rotation c. For the problem to have a solution, we have to make sure that imposed constraints are consistent with each other, i.e., that we are not asking the shape to follow two different tangents at the same point. In practice, we avoid inconsistent constraints by imposing them at different distances from the rotation center, that way they will be propagated along different concentric circles and never contradict each other.

More formally, we define a *proper problem* as one where the distance map $r(\cdot)$ is strictly monotonic, and where the set of constraints change smoothly along the contact curve. Under those conditions the parallel transport of the set of constraints yields a smooth vector field $\mathcal{F}$ defined in an annulus in the plane (Figure 16b). Note that the parallel transport along concentric arcs is a continuous and differentiable operation.

As illustrated in Figure 16c and Figure 16d, an integral curve of that vector field $\mathcal{F}$ satisfies all constraints and solves the scale-invariant problem. The existence of that solution is guaranteed by the theorem of existence and uniqueness of maximal integral curves [72]:

Theorem 1 (Existence and Uniqueness of Maximal Integral Curves)**.** *Let X be a smooth vector field on an open set $U \in \mathbb{R}^{n+1}$ and let $p \in U$. Then there exists a unique and maximal integral curve $\alpha(t)$ of X such that $\alpha(0) = p$.*

6.1 Closed Form Solutions

The construction in the previous section, along with numerical integration, yields a solution to the shape synthesis problem for planar rotational joints. In this section we are interested in finding the analytical expression of the finger shape. As in the previous section, we will assume that the constraints are distributed along a 1-dimensional set, or contact curve $\mathcal{C}$. Besides, we will restrict the analysis to the case where:

- the contact curve $\mathcal{C}$ is a line and,
- the contact vector $\mathcal{V}$ is constant along the contact curve.

We will see in Section 6.2 that this includes the interesting cases of designing effectors with invariant contact properties with respect to the scale or the pose of the object, or any linear combination of both.

Let (x, y) and (r, θ) be the cartesian and polar coordinates in the planar workspace $\mathcal{W}$. The shape of the finger is the solution to the system of first order differential equations:

$$\begin{aligned} \dot{x} &= \mathcal{F}_x \\ \dot{y} &= \mathcal{F}_y \end{aligned} \tag{5}$$

where $\mathcal{F} = (\mathcal{F}_x, \mathcal{F}_y)$ is the vector field constructed in the previous section. Identity (6) relates the derivatives of cartesian and polar coordinates:

$$\frac{dy}{dx} = \frac{r' \sin\theta + r\cos\theta}{r'\cos\theta - r\sin\theta} \tag{6}$$

where $r' = \frac{dr}{d\theta}$. We can then rewrite the cartesian system (5) as the single polar differential equation:

$$\frac{\mathcal{F}_y}{\mathcal{F}_x} = \frac{r' \sin\theta + r\cos\theta}{r'\cos\theta - r\sin\theta} \tag{7}$$

Without loss of generality we normalize the geometry of the problem and suppose that the center of rotation c lies on the X axis, and the contact curve $\mathcal{C}$ is parallel to the Y axis. Let now β be the constant angle between $\mathcal{C}$ and the contact vector $\mathcal{V}$. Depending on the relative location of c and $\mathcal{C}$, there are three cases to analyze:

i. The rotation center c lies on top of $\mathcal{C}$.
ii. The rotation center c is at finite distance from $\mathcal{C}$.
iii. The rotation center c is at infinity, i.e. the finger translates rather than rotates.

6.1.1 Case I: Rotation Center On the Contact Curve

In this case the distance between the center of rotation of the finger c and the contact curve $\mathcal{C}$ is zero. Note that the rock-climbing cam example in Section 1.1 falls into this case, since the contact constraints in Figure 3 have constant direction, and are distributed along a linear segment. We will show now that, indeed, the solution is a logarithmic spiral.

For the purpose of analysis, we place the origin of coordinates at c and the axis Y along the contact curve, as in the diagram in Figure 17a.

In this case, (7) becomes:

$$\frac{\mathcal{F}_y}{\mathcal{F}_x} = \tan\left(\beta + \theta + \frac{\pi}{2}\right) = \frac{r' \sin\theta + r\cos\theta}{r'\cos\theta - r\sin\theta} \tag{8}$$

Solving (8) for r' yields:

$$r' = \frac{dr}{d\theta} = -r\tan\beta \tag{9}$$

Equation (9) is a linear homogeneous ordinary differential equation with general solution:

$$r(\theta) = \mathrm{C}\ e^{-\theta\tan\beta} \tag{10}$$

The solution to the invariant contact problem for case I is a logarithmic spiral with pitch $\frac{\pi}{2} + \tan^{-1}(\cot\beta)$, which we could have anticipated from Figure 17a where we see that the angle between the contact vector and the radial line (line from origin to the finger) is constant. This is characteristic of logarithmic spirals and gives them their scale-invariant properties [71], as we will further see in Section 6.2.

Note that when the angle β reaches one of the limit values $\pm\frac{\pi}{2}$, the logarithmic spiral degenerates into a straight line, caused by the contact vector becoming parallel to the contact line.

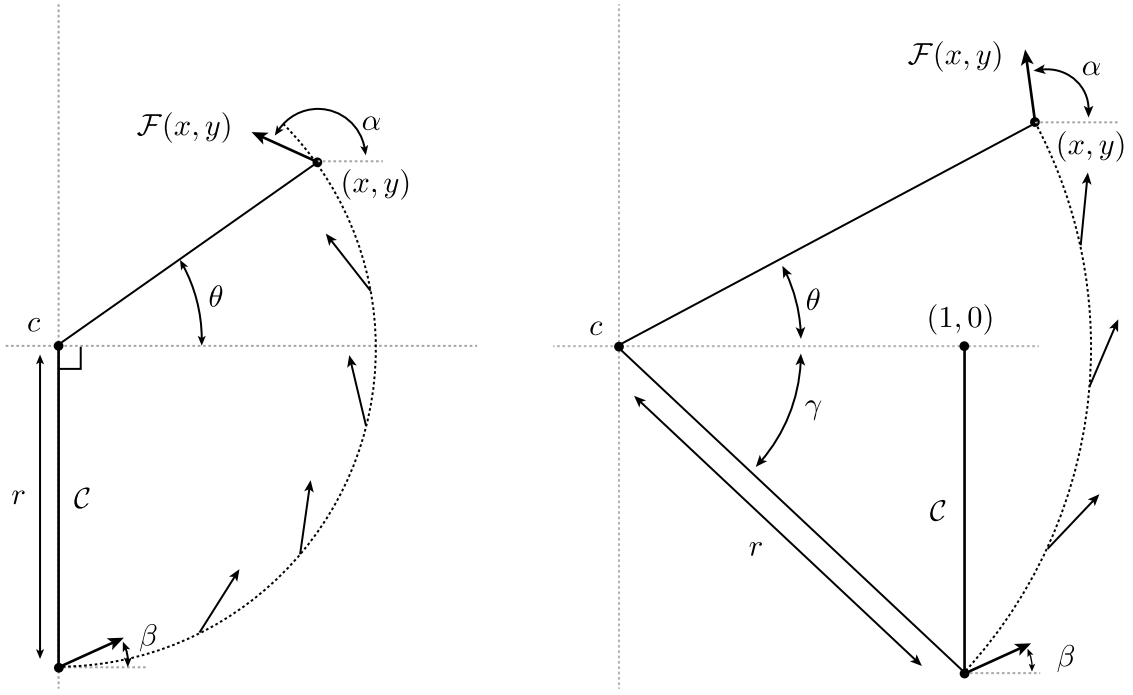

(a) Case I

(b) Case II

Figure 17: Normalized diagrams of the contact geometry for shape synthesis problem when the contact curve $\mathcal{C}$ is a segment and the contact vector is constant along it. (a) Diagram for Case I: the parallel transport of the contact vector along an arc with center c gives $\mathcal{F}(x,y)$, the direction of the vector field at (x,y). Note that the output angle α is $\beta+\theta+\frac{\pi}{2}$. (b) Diagram for Case II: the parallel transport of the contact vector along an arc with center c gives $\mathcal{F}(x,y)$, the direction of the vector field at (x,y). Note that the output angle α is $\beta+\theta+\gamma$.

6.1.2 Case II: Rotation Center at Finite Distance from Contact Curve

In this case the rotation center c is at finite distance from the contact curve $\mathcal{C}$. Without loss of generality we scale the geometry of the problem again so that the distance is unity. As in the previous case, we place the origin of coordinates at c. Now the contact line is vertical and crosses the X axis at $(1, 0)$, as in the diagram in Figure 17b. Equation (7) becomes:

$$\frac{\mathcal{F}_y}{\mathcal{F}_x} = \tan(\beta + \theta + \gamma) = \tan\left[\beta + \theta + \cos^{-1}\left(\frac{1}{r}\right)\right] = \frac{r' \sin\theta + r\cos\theta}{r'\cos\theta - r\sin\theta} \tag{11}$$

After some trigonometric algebra (11) can be solved for r' as:

$$r' = \frac{dr}{d\alpha} = r \cdot \frac{\cos\beta - \sqrt{r^2-1}\sin\beta}{\sin\beta + \sqrt{r^2-1}\cos\beta} \tag{12}$$

Equation (12) is a separable differential equation of the form $\frac{dr}{d\theta} = g(r)$, which can be solved as $\theta(r) = \int d\theta = \int \frac{1}{g(r)} dr$, with the change of variables $t \to \sqrt{r^2-1}$:

$$\begin{aligned}
\theta(r) &= \int \frac{1}{r} \cdot \frac{\sin\beta + \sqrt{r^2-1}\cos\beta}{\cos\beta - \sqrt{r^2-1}\sin\beta}\, dr = \\
&= \int \frac{t}{t^2+1} \cdot \frac{(\sin\beta + t\cos\beta)}{(\cos\beta - t\sin\beta)}\, dt = \\
&= -\int \frac{1}{t^2+1} + \frac{\cos\beta}{\sin\beta t - \cos\beta}\, dt = \\
&= -\tan^{-1}(t) - \frac{\ln(|\sin\beta t - \cos\beta|)}{\tan\beta}
\end{aligned} \tag{13}$$

As illustrated in Figure 18, (13) yields the β-parametrized family of spirals:

$$\theta(r) = -\tan^{-1}\left(\sqrt{r^2-1}\right) - \frac{\ln\left(|\sin\beta\sqrt{r^2-1} - \cos\beta|\right)}{\tan\beta} + \mathrm{C} \tag{14}$$

The solution is valid for all possible values of β except when $\tan\beta = 0$, in which case a similar derivation yields the solution:

$$\theta(r) = -\tan^{-1}\left(\sqrt{r^2-1}\right) + \sqrt{r^2-1} + \mathrm{C} \tag{15}$$

6.1.3 Case III: Rotation Center at Infinity

In this case the center of rotation c is located at infinity, equivalent to a translating or prismatic finger. The vector field $\mathcal{F}$ is in this case generated by the parallel transport of the set of contacts along parallel lines oriented with the direction of translation. The obtained vector field is independent of the direction of translation. $\mathcal{F}$ is constant across the entire plane and oriented with β except in the singular case when the direction of translation is parallel to the contact line. In that case the vector field is only defined on top of the contact line, and the problem is ill-defined.

The integral curve of the induced vector field $\mathcal{F}$ is in this case a line segment aligned with the constant contact vector $\mathcal{V}$, yielding straight fingers. In the degenerate situation of the direction of translation being aligned with the contact line, the solution only exists if the contact vector is also aligned with the contact line, in which case the integral curve is also a straight line segment.

6.1.4 Family of Solutions

Here we summarize the family of closed form solutions to the scale-invariant contact problem for the cases where the contact curve is a line, and the contact vector is constant along it. Figure 18 illustrates the solutions for cases I, II, and III, for different values of β. Note that the vector fields obtained with β and $\beta + \pi$ have the same magnitude and opposite direction, hence it suffices to analyze the range $\left[\frac{\pi}{2}, -\frac{\pi}{2}\right]$. Note also that Figure 18 shows a long section of the spiral. However, for practical reasons, the actual shape of the effector would be just a small portion.

In cases I and II, the integral curve of the vector field is a spiral, with the exception of a few degenerate situations where the integral curve is a line segment or a circle. We make special note of case I with $\beta = 0$ where the contact vector is perpendicular to the contact line. This produces an impractical circular finger that only meets one of the constraints, while, at the same time, does not violate any of the rest. In case III, we always obtain a line segment.

6.2 Application: Grasp Invariance

In this section we introduce *grasp invariance*, a principle to guide the design of finger shape to accommodate variations over shape and/or pose of an object. In the following subsections, we describe three example applications of the principle: A gripper yielding invariant contact geometry with respect to the scale of an object (Section 6.2.1); a gripper yielding invariant contact geometry with respect to the location of an object (Section 6.2.2); and a pick-up tool designed to grab objects from a flat surface (Section 6.2.3).

6.2.1 Scale-Invariant Grasping

The solution to the scale-invariant contact problem in Figure 16 yields a finger with invariant contact geometry for a disk of varying size. Two such fingers add up to a gripper whose equilibrium grasps are geometrically invariant with scale. Suppose we aim for an equilateral triangular grasp between two fingers and a palm. Figure 19a shows the corresponding contact curve $\mathcal{C}$ and contact vector. After normalizing the geometry of the problem as in Section 6.1, we get the diagram in Figure 19b. The solution belongs to the family of spirals in Case II in Section 6.1.2, where the center of rotation is at finite distance from the contact line.

The contact curve, the contact vector, and the form of the finger depend on the object O and the type of contact we aim for. Hence, the form of the finger depends on the task to solve. For the specific example of a disk and the triangular grasp in Figure 15a, we can construct a scale-invariant gripper by combining two identical but symmetric fingers as in Figure 21a.

6.2.2 Pose-Invariant Grasping

Here we aim to design a hand whose grasps are invariant with respect to the location of a given object rather than its scale. Suppose again that we want to grasp a disk of a given size with a triangular grasp, against a planar palm. Now, the disk can be located anywhere along the palm, and we want the grasp geometry to be invariant with respect to that displacement. Figure 20a shows the corresponding contact curve $\mathcal{C}$ and contact vectors, and Figure 20b the normalized diagram. Since the rotation center is at finite distance from the contact line, the solution belongs to the family of spirals in Case II in Section 6.1.2.

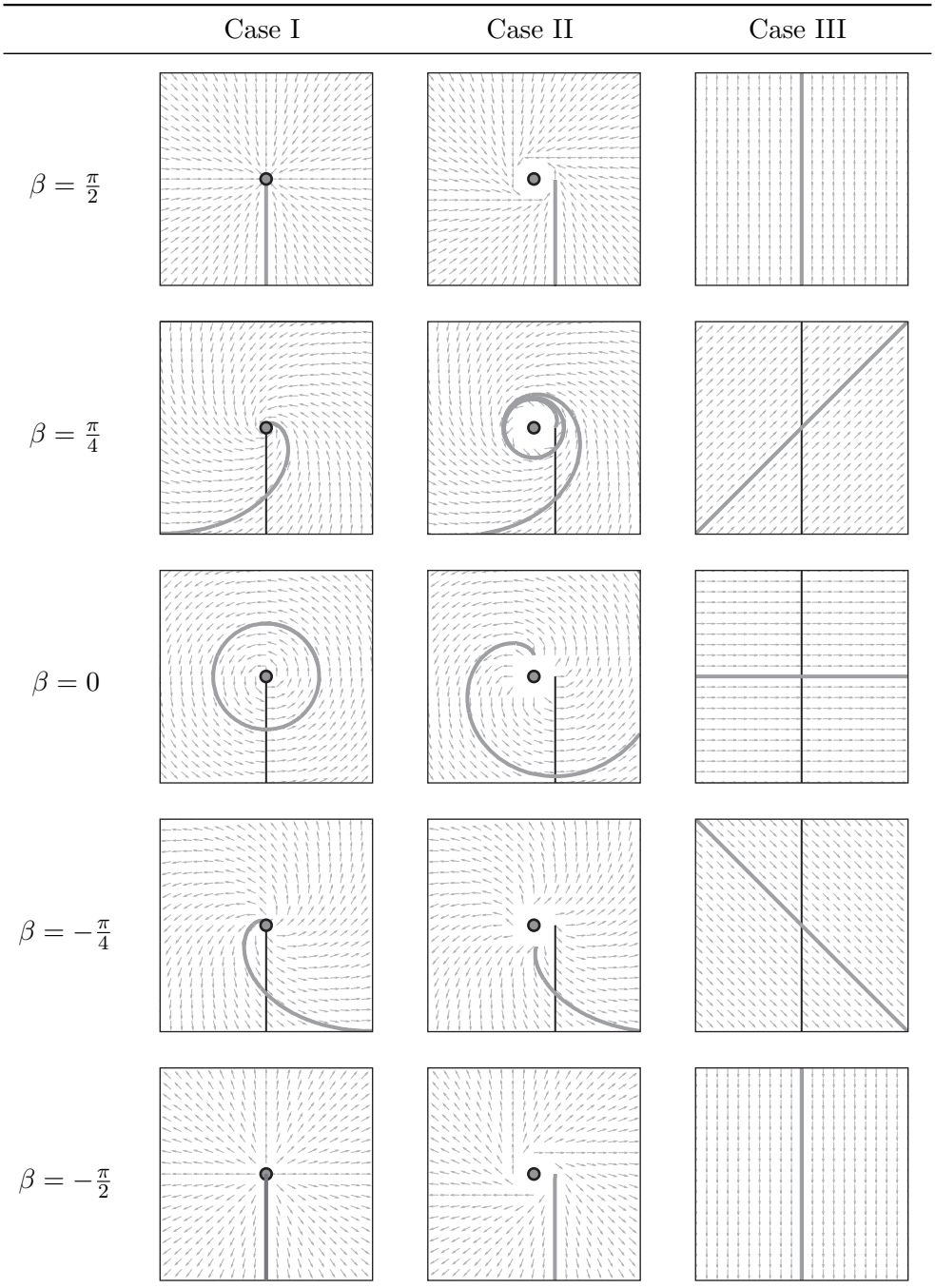

Figure 18: Plots show the contact curve (*vertical bold line*), the rotation center (*grey dot*), and the finger solution (*grey curves*) for different values of β. The finger always crosses the lower half of the contact curve with constant angle β. Case I: Rotation center on the contact curve. Case II: Rotation center at finite distance from the contact curve. Case III: Rotation center at infinity.

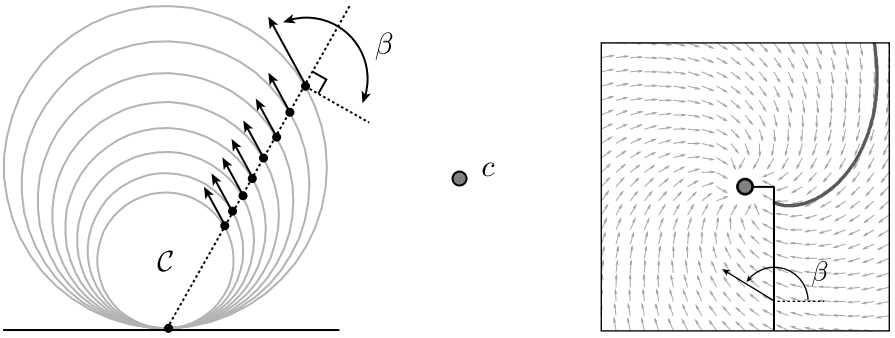

(a) (b)

Figure 19: (a) Contact curve $\mathcal{C}$ and contact vector defining the fingers of a scale-invariant gripper. (b) Corresponding normalized diagram with contact angle β.

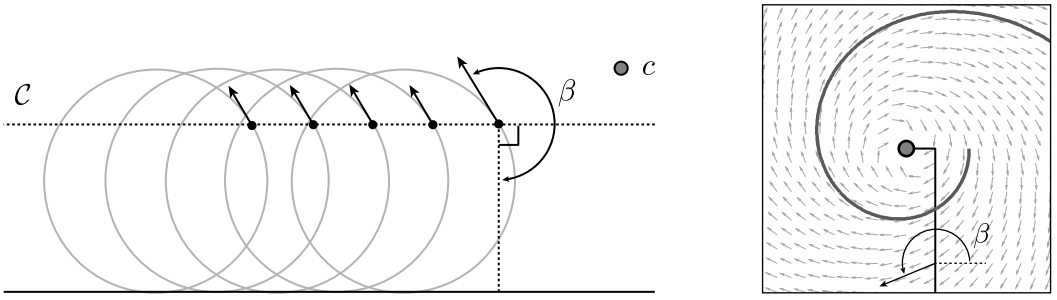

(a) (b)

Figure 20: (a) Contact curve $\mathcal{C}$ and contact vector defining the fingers of a pose-invariant gripper. (b) Corresponding normalized diagram with contact angle β.

Again, the contact curve, the contact vector, and consequently the form of the finger depend on the object O and the type of contact desired. In Figure 21b two identical but symmetric fingers compose a pose-invariant gripper.

6.2.3 Pick-up Tool

Suppose now we are to design a gripper with two rigid fingers to pick up an object from the ground. The object needs to slide along the length of the fingers while it is being lifted, similar to Trinkle and Paul's work on dexterous manipulation with sliding contacts [73]. Because of the critical role that contact geometry plays in the sliding motion, complex lift plans can be simplified if the contact geometry between finger and object were to be invariant during the lifting motion. With that in mind, we can use the grasp invariance principle to find the finger shape that preserves a contact geometry suitable for the sliding motion. Figure 22 shows a gripper designed to such task.

7 Case Study: General 1-DOF Planar Actuation

The previous section shows the derivation of exact solutions for rotating and prismatic fingers in the plane. In this section we detail the process for planar effectors driven by more complex mechanisms such as linkages (Rodriguez and Mason [61]). We also discuss how to find numerical/approximate solutions when analytical ones are not available (Section 7.1), and describe an example application to derive fingers that improve the stability of a grasp (Section 7.2).

The formulation of the shape synthesis problem in Section 5 is independent of the driving mechanism. The process to synthesize the shape of an effector follows the same steps as in the case of planar rotational joints: First we construct the loci of the set of constraints and then we find a curve consistent with them. The implementation of both steps is however more involved in the general case than for rotational joints.

Figure 11 and Figure 12 show the motion field and motion orbits for a linkage and an elliptic trammel. In this case both motion field and orbits depend on the configuration of the mechanism t, and so will do the process to transport constraints. Consequently, the locus of a constraint when projected to the orbit space, follows a trajectory different than a motion orbit. In the following section we describe an approximate method to construct the locus of a constraint, and how to integrate the loci to find the shape of the effector.

7.1 Approximate Solutions

A contact constraint (p, η) is an imposition on the effector to locally comply with η at location $p \in \mathcal{W}$ for an unspecified configuration of the mechanism. The contact constraint is represented in orbit space $\mathcal{O}$ as a locus of constraints $\mathcal{L}_{(p,\eta)} = \{((p_t, 0), \eta_t) : t \in T\}$, where each $((p_t, 0), \eta_t)$ is the shape constraint corresponding to propagate η to configuration $t = 0$ through the motion orbit that crosses p at configuration t.

This means that to construct the locus of a contact constraint, we need to propagate it through infinite motion orbits, each yielding a point in the locus. In practice, since we are working in low dimension—dimension of workspace $\mathcal{W}$ is 2 or 3 and the actuation dimension of the driving mechanism is 1—we can discretize the configuration space of the mechanism and

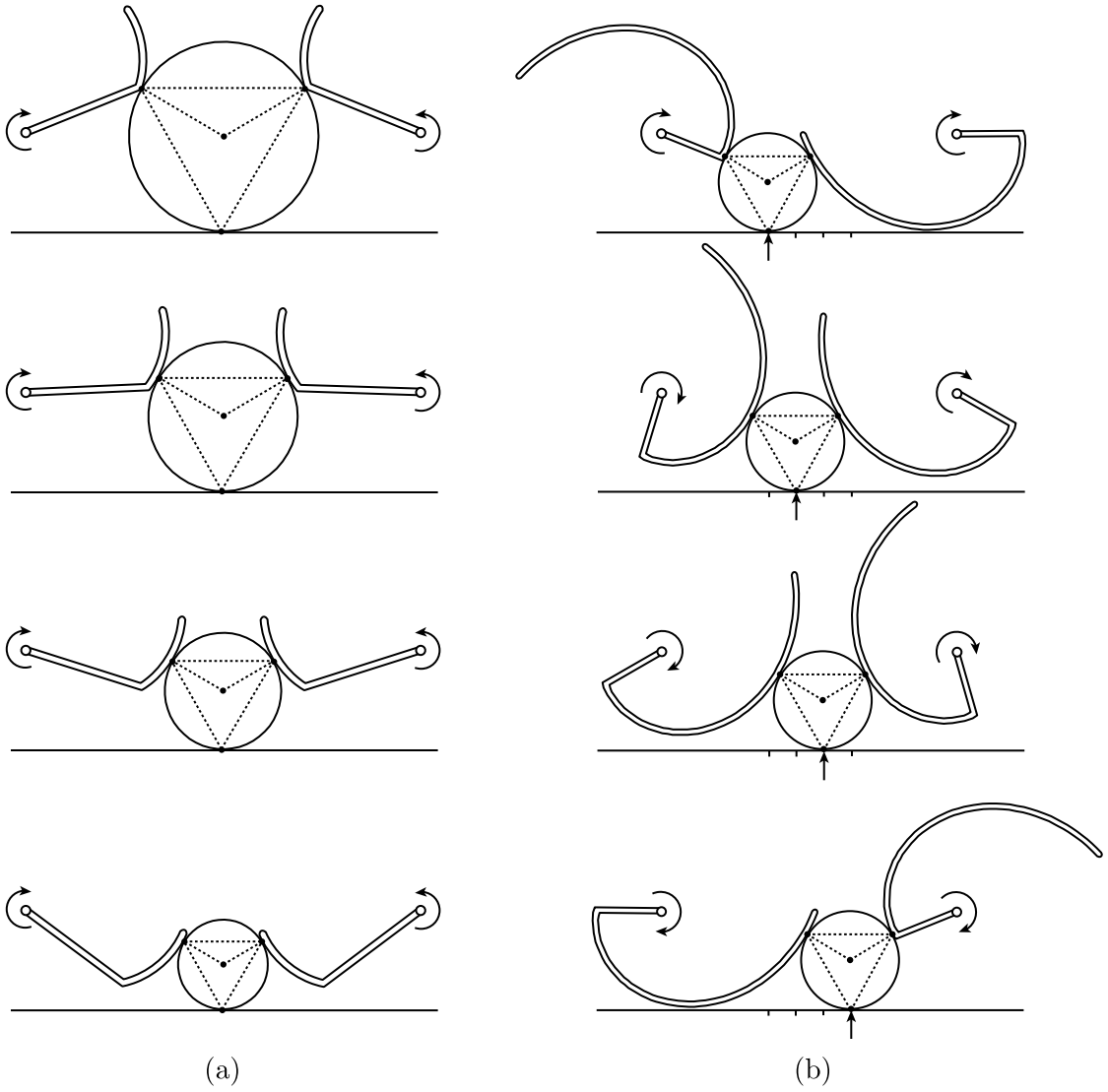

Figure 21: (a) The solution to the scale-invariant contact problem in Figure 19b yields a finger with invariant contact geometry for a disk of varying size. Two such opposing fingers add up to a gripper whose equilibrium grasps (triangular grasp in the figure) are geometrically invariant with the scale of the disk. (b) Analogously we derive the shape of the fingers that yield equilibrium grasps geometrically invariant with respect to the location of the disk.

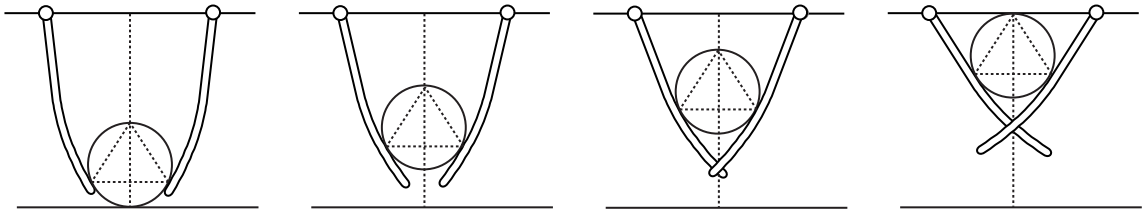

Figure 22: Gripper designed to pick up disks from the ground. The shape of the fingers is design to provide an invariant contact geometry with the disk's lifting motion.

construct a discretized version of the locus. The process is illustrated in Section 7.2 with the example task of designing the phalanges of fingers to improve the stability of a grasp.

Once the loci of all contact constraints is constructed, as in Figure 25a, the second step is to find a curve that is compliant with it. We showed in Section 6 that for the case of a rotational joint and a proper problem, the locus of different contact constraints never cross each other, since they follow concentric circles. In that case, we guarantee not imposing inconsistent constraints by making sure that the distance map to the rotation center $r(\cdot)$ is strictly monotonic. For other mechanisms, that is harder to guarantee.

Following Proposition 1 in Section 4.2, the locus of a constraint follows the motion orbits of the inverted mechanism, which never cross each other in the extended space $\mathcal{W} \times T$ but can cross each other, and in fact most often do, in their projection to orbit space. If it is the case that the locus cross each other, the propagation of constraints do not define a vector field, and the integral curve might not be defined.

In practice, we find an approximate solution by either first approximating the resulting loci by a vector field and then finding an integral curve, or by choosing a suitable starting point and limit the integration until when inconsistent constraints are being imposed. In the following section we show an example where we use a combination of both. We start by constructing only the part of the locus that we care about (the range of motion of the mechanism that we are interested in), and then we approximate the resulting distribution by a vector field. Note also that, for convenience, we will use in the implementation tangent vectors ω rather than contact normals η.

7.2 Application: Grasp Stability

We apply now the shape synthesis process to derive fingers for a two-fingered planar gripper to improve the stability of a grasp of a disk. We will compare the process for fingers driven by linkages and rotational joints.

To characterize the stability of an equilibrium grasp, we consider the energetic model of stability for a compliant simple gripper described in Mason et al. [41], similar to Hanafusa and Asada [27]. Every suitable hand-pose/object-pose configuration induces some level of grasp energy, supplied by motors and stored in springs. Assuming some dissipative forces, stable configurations of hand/object correspond to minima in that potential energy distribution. The shape of the potential energy in a neighborhood of a stable pose determines how stable it is. That way, sharp narrow wells are less susceptible to be degraded by noise than broad shallow wells, and hence represent more stable grasps.

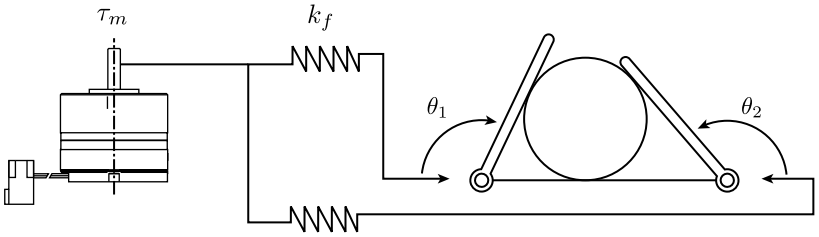

Figure 23: The diagram illustrates the actuation/compliance scheme used to model hand/object interaction. Units are dimensionless throughout the analysis so that the diameter of the disk is 1, the radius of the palm is 1, the constant of finger springs is $k_f = 1$, and when closing the hand, the motor is driven to a stall torque $\tau_m = 1$.

We model the actuation of the two-fingered planar gripper as a constant torque source τ_m compliantly coupled with springs to both fingers (Figure 23), providing a potential energy $U_m = \tau_m \cdot t$, where t is the motor position or actuation parameter. The rest position of the fingers when the actuator is at t is $\theta(t)$. Under compressing forces, each finger provides a potential $U_i = k_f(\theta_i - \theta(t))^2/2$, where k_f is the spring constant of the finger and θ_i is the finger angle. The total energy of a grasp can then be computed as:

$$U = U_m \ + \sum_{i=1}^{2} U_i = \tau_m \cdot t + \ \sum_{i=1}^{2} \frac{1}{2} k_f \left(\theta_i - \theta(t)\right)^2 \tag{16}$$

The shape of the potential energy U depends on the finger-object contact geometry. By choosing different contact locations for different object poses, we can affect the shape of that potential energy and improve the stability. Figure 24a shows a few selected contact points for different locations of a disk, each contact point constituting a contact constraint to satisfy. To increase the stability of a grasp we chose contact points such that:

- Give a stable contact geometry for the desired stable configuration (i.e., central grasp).
- If the object deviates to the left of the stable grasp, the left finger should contact at a new location where it is easy for the finger to push it back to the center and viceversa for the right finger.
- If the object deviates to the right of the stable grasp, the left finger should contact at a new location where it is difficult or impossible for the finger to push the object further away from the center, and viceversa for the right finger.

The problem of choosing contact constraints is key to the mechanics manipulation, but is not the focus of this thesis. For the rest of this section, we assume that we are given the set of desired constraints in Figure 24b.

As per the formalization of the shape synthesis problem in Section 5 we transform the set of contact constraints into their corresponding loci in the orbit space. Figure 25 shows the loci for a finger actuated by a rotational joint and a finger actuated through a Hoekens linkage. To find a solution, we approximate the set of constraints by a vector field and integrate it numerically to find an integral curve. The obtained curve results in an effector that complies with the imposed constraints and sharpens the potential energy wells of the central equilibrium grasp relative to straight fingers (Figure 26).

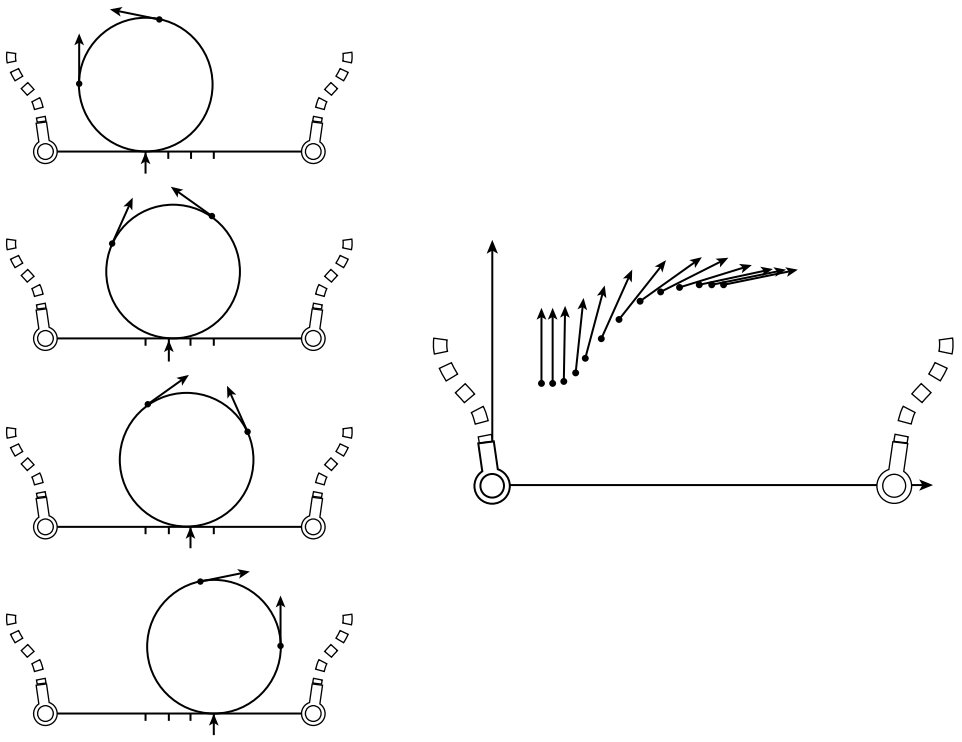

(a) (b)

Figure 24: (a) We chose contact points with the disk so that the left finger can easily push the disk only when it is to the left of the central stable pose. Opposite for the right finger. (b) Denser collection of the contact constraints imposed to the shape of the left finger. That collection is the input to the shape synthesis problem.

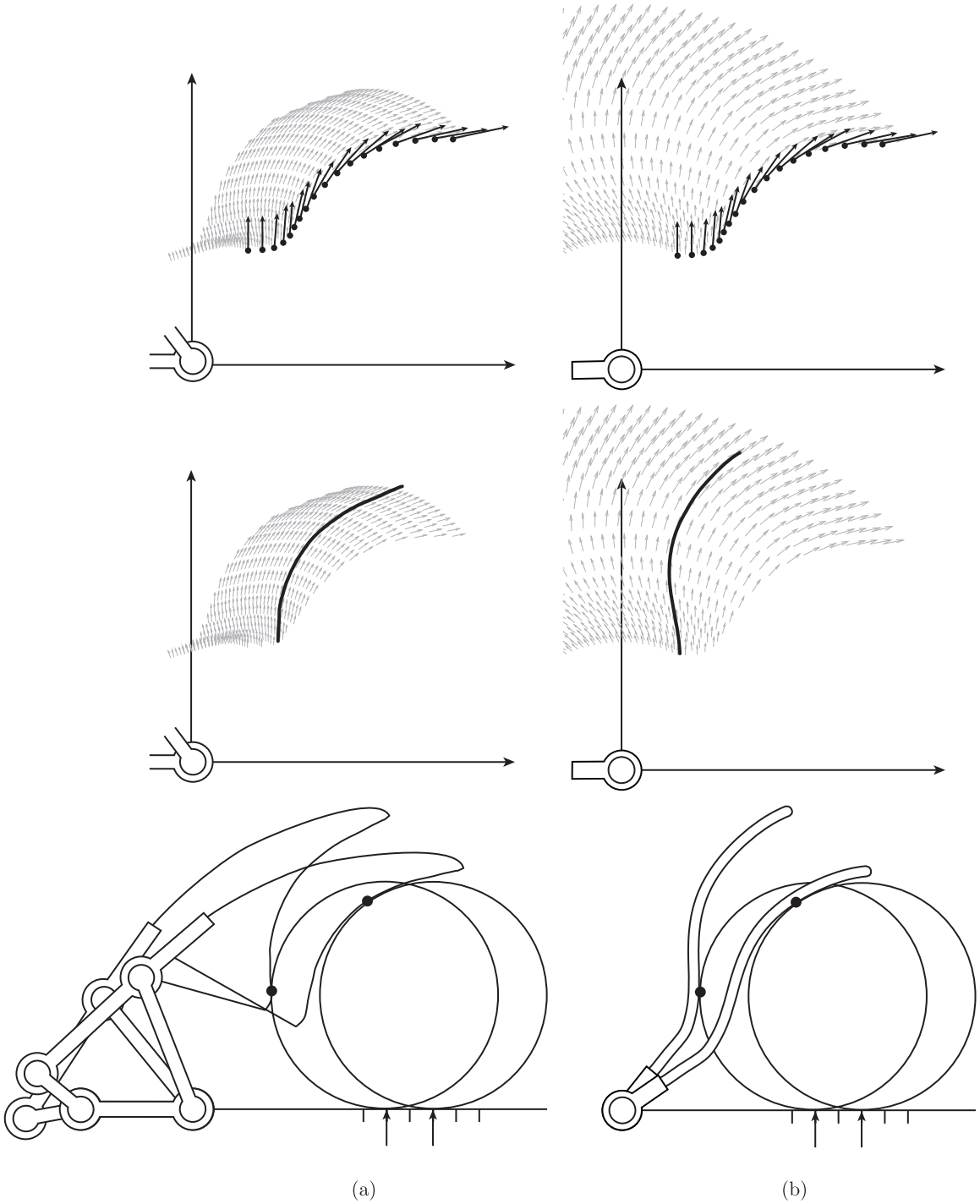

Figure 25: Side by side comparison of the process to design fingers to improve the stability of a grasped disk, when the fingers are actuated by (a) a Hoekens linkage or (b) a rotational joint. The top row shows the loci induced by the constraints in Figure 24. The middle row shows a solution shape of the effector. It was computed numerically by approximating the loci as a vector field and finding an integral curve. The bottom row shows the resulting effectors.

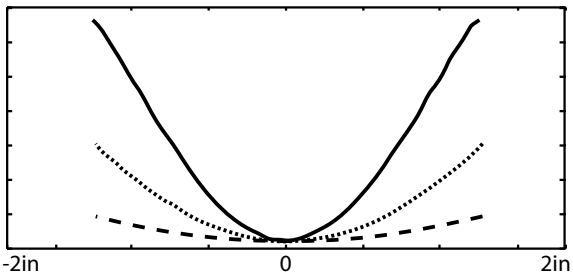

Figure 26: Comparison between the grasp energy induced by fingers designed for a Hoekens linkage (solid line), designed for a rotational joint (dotted line), and straight fingers with a rotational joint (dashed line). To enable the comparison, in each case we have zeroed the energy of the grasp configuration with minimal energy.

Note that Figure 25 shows two different effector shapes actuated by two different mechanisms and produce the same contact pattern with the object. To some degree, this illustrates the importance of shape. The selection of shape is critical to the final interaction of the effector with the object, even to the point where, with the appropriate shape, a complex mechanism like a linkage can be "emulated" with a simpler rotational joint.

8 Case Study: General 1-DOF Spatial Actuation

In this section we discuss differences and similitudes in the shape synthesis problem between the planar and spatial cases. The most consequential difference is that, in the spatial case, the shape of the effector is a surface while in the planar case is a curve:

- One one hand, this makes the problem more complex. Tangent vectors become tangent planes, which are more difficult to impose and integrate than vectors.
- One the other hand, it opens the door to a larger utilization of shape. It gives us the opportunity to extract more functionality out it.

We showed in Section 4.1 that the domain of influence of contact constraints are motion orbits. Combined with the need to avoid inconsistent constraints, it implied that for 1-DOF planar effectors we could only impose a 1-dimensional family of constraints. That is the case for all examples described so far, from the rock-climbing cam in Section 1 to the grippers in Section 6 and Section 7. In particular, we have seen that in the case of rotational joints, for the solution to be fully and uniquely determined, the 1-dimensional set of contacts must be imposed at strictly monotonic distances from the location of the rotational joint.

The spatial case is analogous. If we want to avoid inconsistent constraints, we can only impose one contact per motion orbit. A surface in 3D, however, is fully determined by a 2-dimensional set of tangent planes, rather than a 1-dimensional set of tangent vectors. We will see in Section 8.2 that this means we will be able to impose more constraints. In practice, we will benefit from it by using different "facets" of the finger for different purposes.

Constraint propagation works the same way as in the planar case. The formalization of the motion model of an effector, described in Section 3, is independent of the workspace dimension.

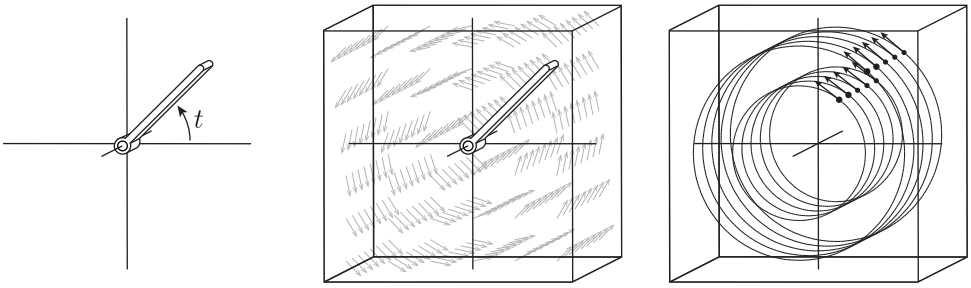

(a) (b) (c)

Figure 27: Motion model of a spatial rotational joint. (a) Rotational joint in a 3 dimensional workspace. (b) The motion field is constant along the axis of rotation. As in the planar case, the motion field is independent of the configuration of the mechanism t. (c) The motion orbits projected to the workspace are concentric circles in $\mathbb{R}^3$. Notice that now there is a two-dimensional set of motion orbits.

The motion field $\mathcal{M}$ of a mechanism for a workspace point p and mechanism configuration t is defined as the direction of imposed effector motion, $\mathcal{M}(p,t) = \left(\frac{\partial E(s,t)}{\partial t}, 1\right)$, which now is of higher dimension than in the planar case, but as illustrated in Figure 27a and Figure 28a, still has the form of a vector field.

Also analogous to the planar case, motion orbits are the integral curves of the flow of the motion field, that is, the trajectories in $\mathcal{W}\times T$ followed by possible effector particles. Figure 27b and Figure 28b show the projection of those motion orbit to the workspace for two examples of spatial actuators.

In the following sections we will see ideas of how to handle tangential surface constraints, specially in the integration step of the shape synthesis problem (Section 8.1) and an application to design the fingers of the MLab Hand (Section 8.2).

8.1 Spatial Integration

In the formulation the shape synthesis problem, we have represented contact constraints by the normals we expect the effector to provide. Using contact normals η is convenient formulation-wise. We do not need to make distinctions between the planar and spatial cases. Implementation-wise, however, it will be more convenient to represent contact constraints as tangents vectors or planes.

In the case of a spatial effector, this means representing each contact as two independent vectors spanning the corresponding tangent plane. A set of desired contact constraints then induces two independent vector fields, one for each tangent direction. For the surface of the effector to be a solution, it must be tangent to both.

The construction of the loci is identical to the planar case, except that we must repeat the process twice, once for each vector defining the tangent plane. In the simpler case of spatial rotational joints, where motion orbits never cross in the workspace, the loci of a set of constraints is represented in the orbit space by two vector fields defined in a cylindrical annulus oriented with the axis of the rotational joint.

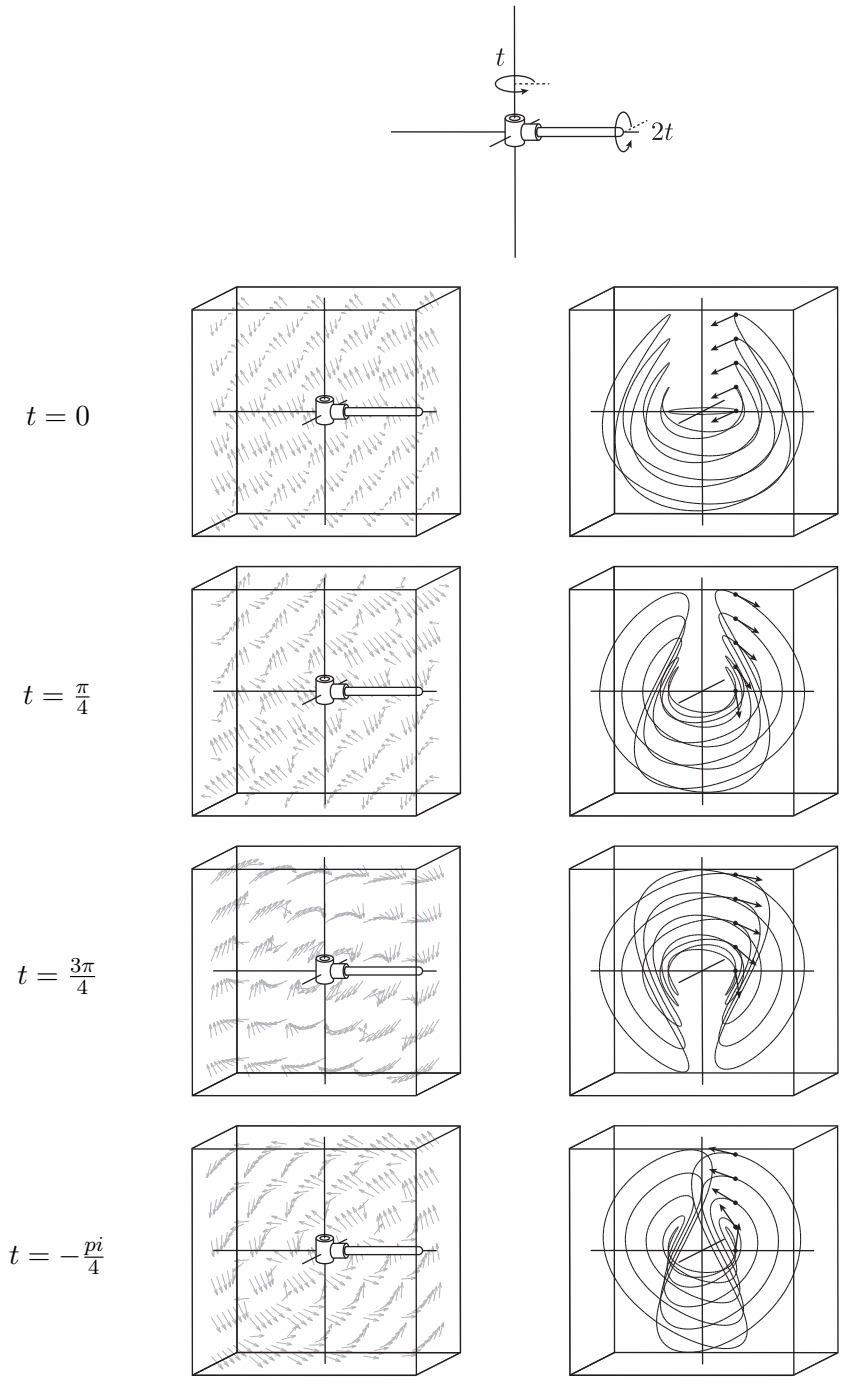

Figure 28: Motion model of a double rotational joint. This example mechanism composes in series two rotational joints with orthogonal axis. We assume both rotations are synchronized (so that overall is a 1-DOF mechanism), the second with twice the angular velocity of the first one. (left) Motion field for 4 different configurations: $t = 0$, $t = \frac{\pi}{4}$, $t = \frac{3\pi}{4}$, and $t = -\frac{\pi}{4}$. Note that it is dependent on the configuration t. (right) Corresponding motion orbits.

The integration step involves finding a surface that complies with those two vector fields. While it is pretty straightforward to find an integral curve of a vector field, from an integration perspective, it is a bit more involved in the spatial case.

Let $\mathcal{L}_{(p_i,\eta_i)}$ be the loci of a set of normal constraints. Assuming there are no inconsistent constraints, $\mathcal{L}_{(p_i,\eta_i)}(p)$ is a vector representing a contact normal at p. Let $\alpha(u,v) = E(u,v,0)$ be a parametrization of the surface of the effector in orbit space for $(u,v) \in [u_{\min}, u_{\max}] \times [v_{\min}, v_{\max}]$. In a general, α must satisfy:

$$\begin{cases} \dfrac{\partial \alpha}{\partial u} \cdot \mathcal{L}_{(p_i,\eta_i)}(\alpha(u,v)) = 0 \\ \dfrac{\partial \alpha}{\partial v} \cdot \mathcal{L}_{(p_i,\eta_i)}(\alpha(u,v)) = 0 \end{cases} \tag{17}$$

a system of two first-order partial differential equations (PDEs) with two independent parameters u and v. Although it is possible to solve the system using standard techniques for PDEs, in Section 8.2 we use a simpler but more restricted implementation: First, we represent the loci $\mathcal{L}_{(p_i,\eta_i)}$ of contact normals by a couple of independent vector fields $\mathcal{L}_u$ and $\mathcal{L}_v$ both orthogonal to $\mathcal{L}_{(p_i,\eta_i)}$. We then parametrize the solution along the integral curves of $\mathcal{L}_u$ and $\mathcal{L}_v$, in which case the integration becomes analogous to the planar case, where we can approximate the surface solution by iterative 1-dimensional integration of $\mathcal{L}_u$ or $\mathcal{L}_v$ along those preferred directions.

8.2 Application: Grasp Versatility and the MLab Hand

> *"Many robotic hands have been designed and a number have been built."*
> — Nathan Ulrich, *Grasping with Mechanical Intelligence [74].*

The MLab hand is a simple gripper designed in the context of the Simple Hands project in the Manipulation Lab at Carnegie Mellon University. Several prototypes have been produced (Figure 29) and extensively used in different applications, including bin-picking, haptic sensing, and general purpose in-hand manipulation. The goal of the hand is to explore the tradeoff between simplicity and generality in robotic hands (Mason et al. [41]), and to design a simple, inexpensive, robust, and functional gripper.

One of the main reasons to study simple hands is that, being simpler, we can gain a better understanding of the principles guiding the design and control of robotic hands. The Mlab hand is designed following a "let the fingers fall where they may" approach to grasping, where the grasp process is passively controlled by the mechanics of grasp stability and is continuously informed by learned stochastic models of haptic sensing. Several features of the hand have been studied and optimized. In this section we describe efforts in the design of the shape of its phalanges.

For the purpose of this thesis, it is enough to know that its design follows these guidelines:

- A flat low-friction palm. Low friction produces a small number of stable poses for a general object within the hand.
- Three fingers arranged symmetrically around a palm, and compliantly coupled to a single actuator. The actuation model approximates the model depicted in Figure 23.
- Deliberately shaped phalanges.

Figure 29: Series of prototypes of the MLab Hand. In Section 8.2 we show examples of fingers designed for P3 and P3.5.

The main goal in this section is to explore the role of the rigid fingers of the MLab Hand as contacting surfaces to provide good grasps for a wide variety of objects and grasp types. In particular we will show that, although the gripper is driven by a single actuator, it can accomodate most grasp types identified in grasp taxonomies, and reproduce a large fraction of the most common grasps used by other more complex hands. Section 8.2.1 gives a brief introduction to grasp taxonomies and how they inform hand design. Section 8.2.2 and Section 8.2.3 show examples of plannar and spatial fingers derived for the MLab Hand.

8.2.1 Grasp Taxonomies

Robotic hand design has been dominated in the last decades by three different principles [41]: anthropomorphism, in-hand manipulation, and grasp taxonomies.

Anthropomorphism aims directly at emulating the human hand. Humans are skilled manipulators; surely part of that skill must come from the mechanism itself. There are several reasons why replicating the human is a good idea, including the impressive manipulation capabilities of humans, and the anthropic nature of environments where robots need to operate. The downside is that it often yields complex designs difficult to use and understand.

In-hand manipulation is the process of controlled repositioning of an object in the hand, often using its fingers. The design of robotic hands to enable general purpose in-hand manipulation follow from knowledge of the mechanics of manipulation, for example by advising on practical requirements like the number and location of contacts needed to stably manipulate an object, or the amount of control needed over each one of them (Okada [48], Salisbury and Craig [65], Brock [8], Bicchi et al. [4]).

Finally, grasp taxonomies describe "distinctively" different hand configurations commonly used to hold and use objects. Robotic hand designs informed by human grasp taxonomies try to reproduce the poses and contact configurations taken by humans rather than directly its mechanical structure. Several grasp taxonomies have been produced over the years (Schlesinger [67], Cutkosky [16], Napier and Tuttle [46]).

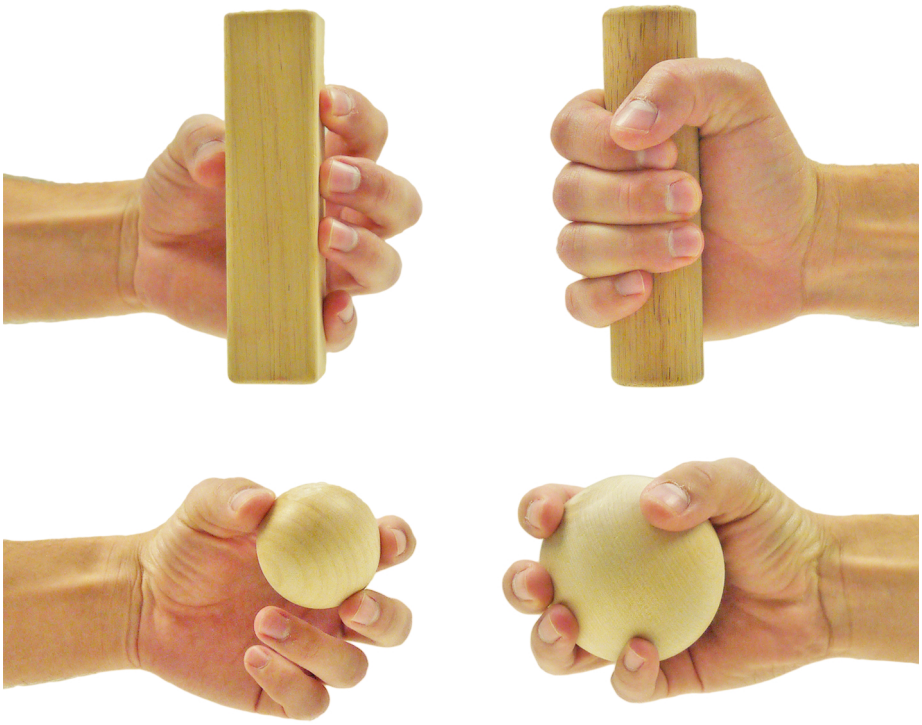

Figure 30: Examples of fingertip vs. enveloping grasps (columns) and prismatic vs. circular grasps (rows).

Most taxonomies identify two broad classes of grasps: *enveloping* and *fingertip* grasps (Figure 30). In enveloping grasps, larger parts of the surface of the hand (mostly finger and palm) are in contact with the object to provide a more firm or powerful grasp. Fingertip grasps, on the other hand, are usually achieved with the fingertips of the fingers to provide a more controlled and accessible grip. Both types are used for very different tasks, and a general purpose hand should be capable of both.

Another useful characterization commonly seen in grasp taxonomies, orthogonal to the distinction between enveloping and fingertip grasp, is the distinction between circular and prismatic grasps [16] (Figure 30). Circular grasps are adequate for spherical and disk shaped objects, and prismatic grasps are adequate for cylindrical and prismatic objects. While the enveloping/fingertip characterization refers mostly to the location of the object in the hand, the circular/prismatic distinction refers to its shape.

Inspired by those characterizations, we will demonstrate the techniques developed in this thesis by designing fingers to recreate those grasp types. In particular, we will design the shape of the phalanges of the MLab Hand to accomodate geometrically correct grasps of spheres, cylinders, and prisms of varying size both in enveloping and fingertip configurations.

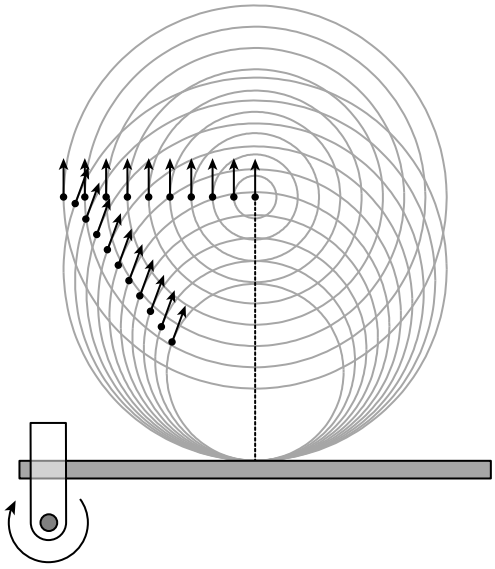

Figure 31: Set of imposed contacts. They will enable the hand to grasp spheres of varying size both in enveloping and fingertip configurations.

8.2.2 Fingers of the MLab Hand: Planar Example

Before designing the 3D shape of the fingers of the MLab Hand in the following section, here we show a simpler and easier to visualize example where we derive fingers to accomodate grasps of spheres of varying size both in enveloping and fingertip configurations. The fingers need to satisfy a 1-dimensional set of geometric constraints. Consequently, it is enough to look at the fingers as actuated by planar rotational joints and simply design the curved profile along their length.

The problem is described more precisely in Figure 31. We impose contact constraints so that the hand is capable of providing geometrically correct grasps of spheres (disks in the plane) of varying size both in fingertip and enveloping configuration. There are multiple options to chose how and where to grasp the targeted spheres. The only restriction is to chose contacts so that the induced constraints are imposed at monotonically increasing distances from the rotation center, which will guarantee the existence of solution.

The combination of all those constraints defines the shape of the finger. It is key to notice that we use two different regions of the finger surface to provide different grasp types (distal part of the phalange for fingertip grasps and proximal part for enveloping grasps). This is something we will further exploit in the following section. In this case the proximal and distal sections of the finger are used to provide geometrically invariant grasps of spheres respectively in enveloping and fingertip configurations.

Figure 32 illustrates the generation and integration of the loci of the imposed constraints, as well as the final shape. In Figure 33 we see the MLab hand grasping differently sized spheres accordingly to the planed contact geometry.

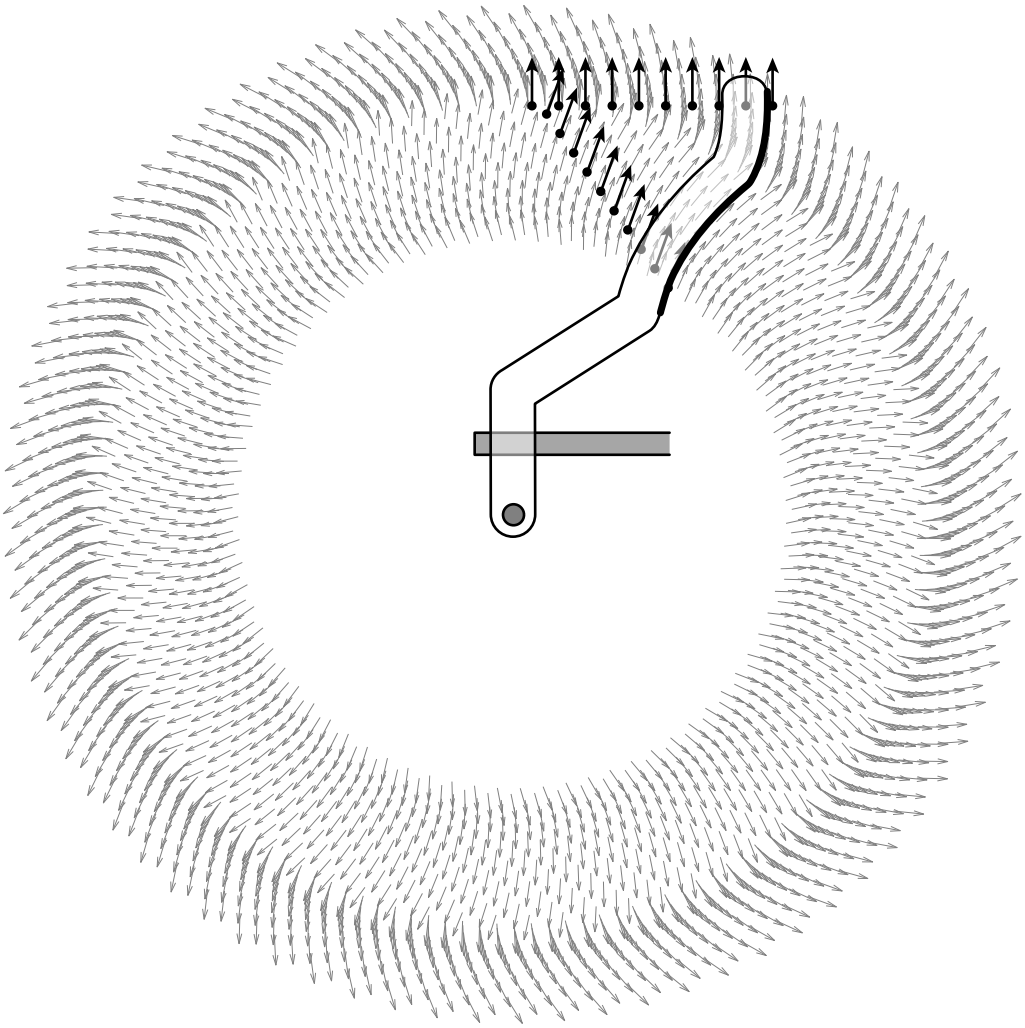

Figure 32: We find a solution by constructing the loci of the set of constraints in Figure 31 and integrating the resulting vector field.

Figure 33: Fingertip and enveloping grasps of differently sized spheres.

8.2.3 Finger of the MLab Hand: Spatial Example

We proceed now to design the 3D shape of the fingers of the MLab Hand. The desired functionality is described in Figure 34 in terms of the set of surface contacts we want the hand to recreate.

The goal is for the hand to be able to grasp spheres and cylinders of varying size both in enveloping and fingertip configurations, as well as two-fingered pinch grasps of prisms of different size. These are described in Figure 34 with illustrative examples of the resulting grasps and the set of surface contacts imposed to yield the desired grasp geometry. As in the planar example in Section 8.2.2 we chose the constraints so that they do not interfere with each other. In practice, this means that different regions of the finger surface will provide the necessary contacts for the different grasp types. Those surface "patches" are shown overlaid on top of the final finger design in Figure 36.

Figure 35 shows the loci induced by the set of contact constraints in Figure 34, as well as the shape resulting from integrating it. Figures 37, 38, and 39 show some examples of the resulting grasps of the MLab Hand. In particular they show how the contact geometry changes with the scale of the object, for the example cases of enveloping grasps of spheres, fingertip grasps of cylinders, and pinch grasps of prisms. In all cases, the obtained contact geometry is in accordance with the planned one.

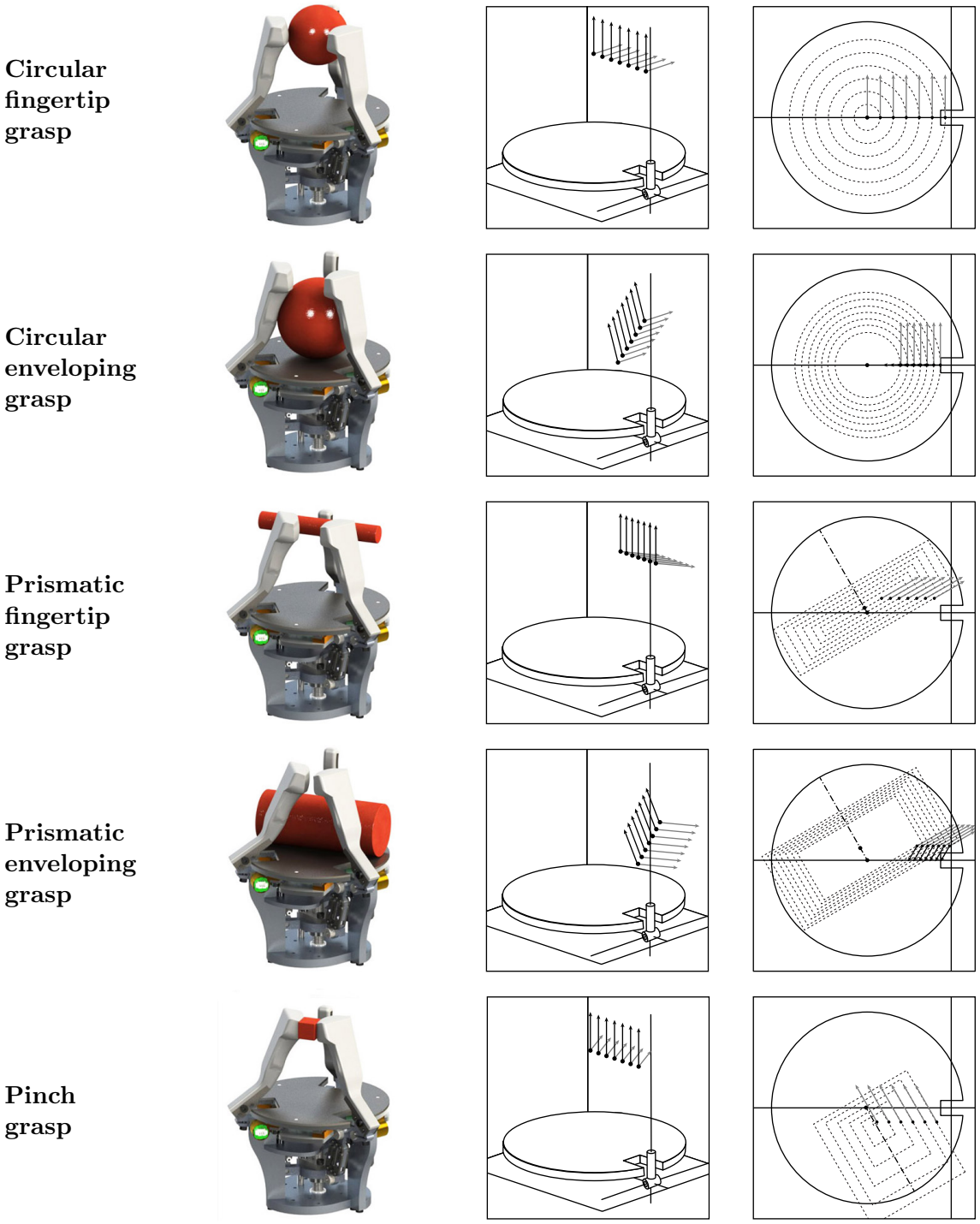

Figure 34: Five grasp types that we want the MLab Hand to execute: fingertip and enveloping grasps of spheres of varying size, fingertip and enveloping grasps of cylinders of varying size, and pinch grasps of prisms of varying size. The first column shows an example of the resulting grasp we want to enable. The second and third columns show the side and top view of the set of imposed contacts, each a dupla of orthogonal vectors spaning the correspondent tangent plane.

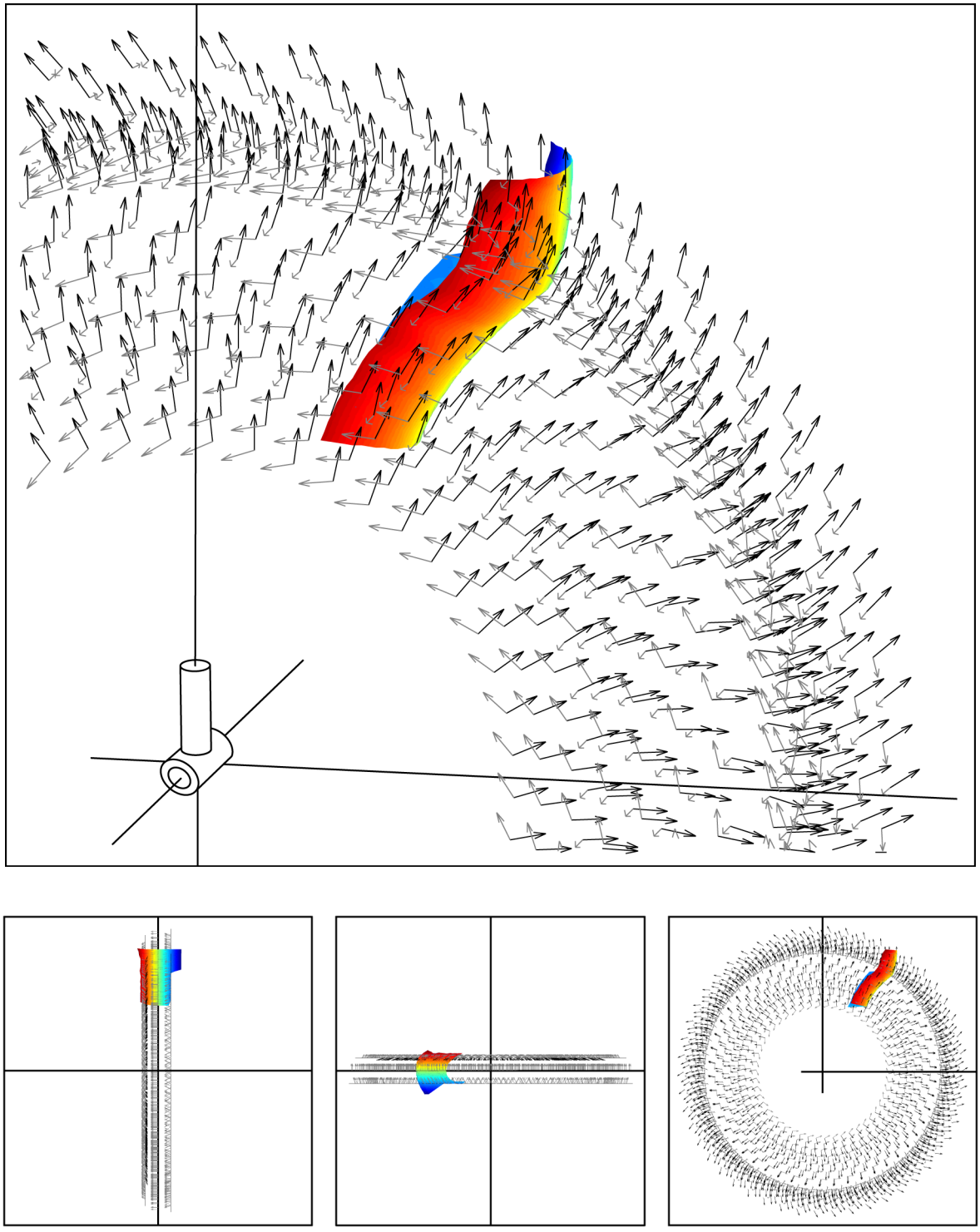

Figure 35: Loci induced by the set of constraints in Figure 34. We integrate the loci to obtain the shape of the phalanges of the MLab hand, better illustrated in Figure 36. The bottom row show the rear, top, and side views of the loci and surface solution.

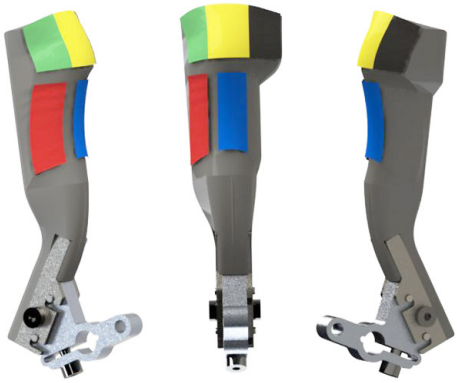

Figure 36: Integrated finger shape, ready to be attached to the MLab Hand. The figure illustrates three views of the different contact regions in the surface of the finger. From left to right, top to bottom, the regions correspond to: (green) fingertip grasps of cylinders; (yellow) fingertip grasps of spheres; (black) pinch grasps of prisms; (red) enveloping grasps of cylinders; and (blue) enveloping grasps of spheres. The central patches for grasping spheres follow the same profile as the solution to the planar case in Figure 32. The patches are singled out for visualization purposes, but they emerge from a single integration of the set of all constraints in Figure 34. Their location in the finger can be manually tunned when defining the desired contacts.

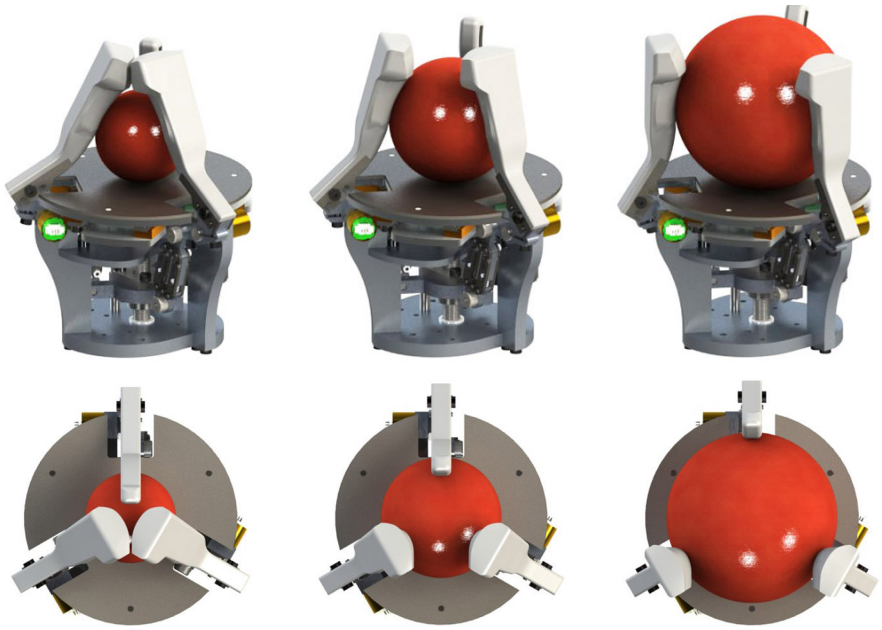

Figure 37: Enveloping grasps of spheres of radius 0.75in, 1.125in, and 1.5in. The radius of the palm is 2in.

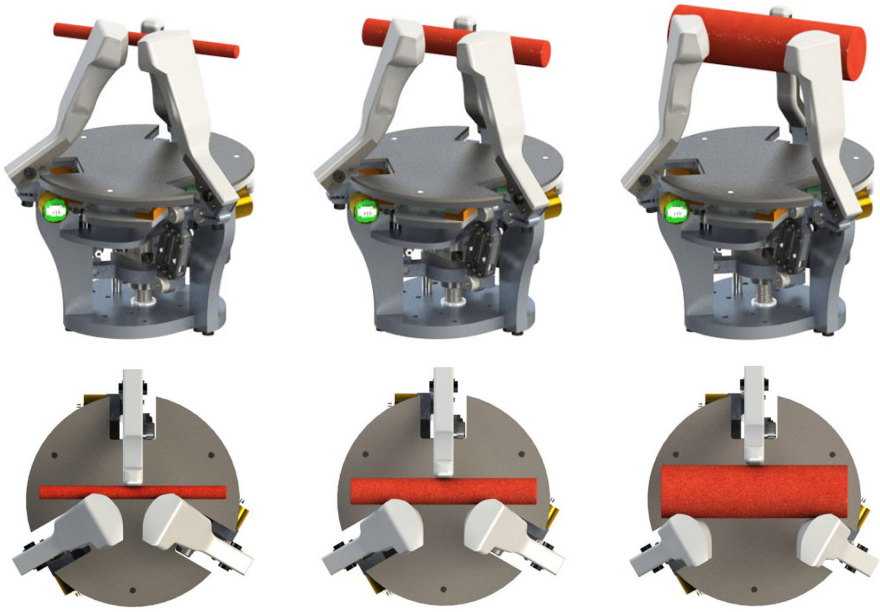

Figure 38: Fingertip grasps of cylinders of radius 0.125in, 0.25in, and 0.5in. The radius of the palm is 2in.

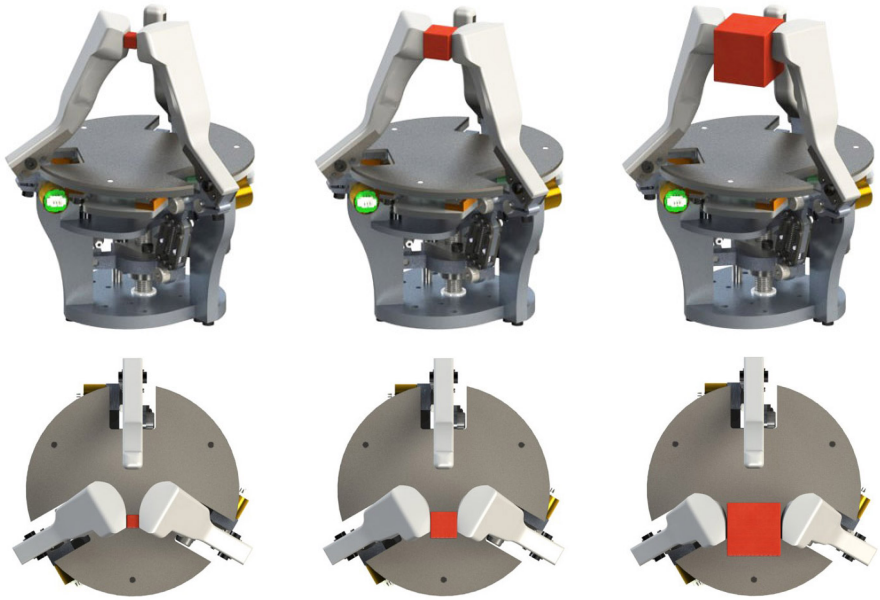

Figure 39: Two-finger pinch grasps of prisms of side length 0.25in, 0.5in, and 1in. The radius of the palm is 2in.

9 Discussion

This thesis is an exploration of shape as a design freedom. Several are the reasons that motivate the study of shape:

- Shape is *relevant* to manipulation. It plays a key role in determining the reaction to contact. In particular, in this thesis, we are interested in the role played by shape in determining contact geometry, and how that can be used to guide the interaction between effector and object;
- Shape is *cheap*. It can be used to increase the capabilities of simple effectors without increasing their complexity or needs for control. Alongside other mechanical attributes like compliance or underactuation, it can convey mechanical intelligence. From a fabrication perspective, the uprise of additive manufacturing and rapid prototyping techniques, makes it simple and inexpensive to fabricate 3D complex geometries on demand;
- Shape is *unavoidable*. Design choices have consequences, and when designing a mechanism we are always forced to chose a shape. We might as well take an informed decision.

In this thesis we address the problem of synthesizing shape of an effector to accomplish a certain mechanical purpose or task. Most previous work, in part inspired by automation applications like part orienting or assembly, represent mechanical purpose by constraining at will the set of relative configurations between two objects. In that context, shape synthesis can be seen as the inverse of the motion planning problem, where the synthesized shape is meant to void the undesired motion freedoms of an object. In contrast, in this thesis, we represent mechanical purpose directly by imposing a desired reaction to contact between effector and object. The mechanical purpose of an effector is encoded in the contacts and forces that is capable of producing. The main contribution of this thesis is to formalize the problem of synthesizing a shape driven by a given mechanism to produce a desired set of contacts.

We look at an effector as the combination of a driving mechanism and a rigidly attached shape. We represent the motion of the effector by a set of *motion orbits*, or integral curves of a vector field $\mathcal{M}$ in $\mathcal{W} \times T$ representing the direction of imposed effector motion. In turn, motion orbits allow us to formalize *constraint propagation*, the process to transform contact constraints to different mechanism configurations. Constraint propagation yields a representation of contact constraints independent of the mechanism configuration, the *locus* of a constraint, which allows us to overcome the challenge of having to enforce contact contraints for an undetermined configuration of the mechanism.

We illustrate developed techniques with three case studies: planar rotational joints; general 1-DOF planar actuation; and general 1-DOF spatial actuation. We use those case studies to introduce three different principles to guide the design of the phalanges of robotic hands: invariance of contact geometry with respect to the scale or pose of an object; improved grasp stability for a given object and grasp; and increased grasp versatility of a robotic hand. We finally showcase the tools with the design of the fingers of the MLab hand, a simple gripper with three fingers compliantly coupled to a single actuator capable of exerting geometrically correct three-fingered grasps of spherical and cylindrical objects or varying size both in fingertip and enveloping configuration, and two-fingered pinch grasps of prismatic objects of varying size.

We will finish now by discussing some limitation of the formulation, as well as some promising future directions, including the multi-DOF case.

9.1 Multi-DOF Case

The case of mechanisms with more than one degree of freedom is considerably more difficult to address. The configuration space of 1-DOF mechanism is very simple. It is 1-dimensional, and can only be traversed forwards or backwards. The multi-DOF case, however, poses a very interesting challenge: there are infinite many ways to go from configuration A to configuration B, and each one yielding a different contact pattern with the environment. The challenge and the opportunity is that now design and planning are note separable problems. We cannot design a shape for the effector without knowing what plan the effector is going to follow to move from A to B. Likewise, the selection of a plan must be informed by the shape attached to the effector. The design space is larger, which complicates the problem but at the same enlarges the set of problems with solution.

The multi-DOF case is important. Most robotic hands have fingers with more than one phalange, either individually actuated or with some sort of compliant coupling scheme between them. In both cases it would be interesting to have a principled way to undersand the effects of shape in object interaction. The multi-DOF case is also interesting in the context of locomotion. Legs, even simple models, have more than one degree of freedom. It would be interesting to understand the combined effects of gait and foot shape in the interaction with the terrain.

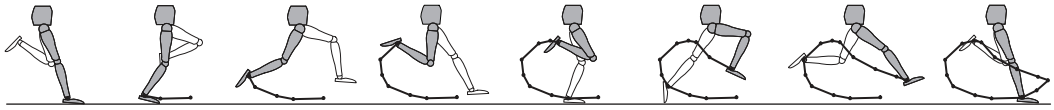

Figure 40: Human running gait. Adapted from Decker et al. [17].

The formalization in this thesis of the 1-DOF case suggests a generalization to the multi-DOF case. For simplicity of notation, we will focus on the 2-DOF case. The configuration space of the mechanism is now parametrized by t_1 and t_2. At each point p in the workspace there are two privileged directions in which the mechanism can advance, one corresponding to each degree of actuation. The motion field becomes a distribution of dimension 2:

$$\mathcal{M} : (p, (t_1, t_2)) \mapsto \left\langle \left(\frac{\partial E(s, t_1, t_2)}{\partial t_1}, (1, 0) \right), \left(\frac{\partial E(s, t_1, t_2)}{\partial t_2}, (0, 1) \right) \right\rangle$$

We use a similar argument than in the 1-DOF case to show that the integral surfaces of the distribution foliate $\mathcal{W} \times T$. Now, equivalent to motion orbits we have 2-dimensional surfaces that represent all points in $\mathcal{W} \times T$ reachable by a point in the surface of the effector. Constraint propagation and the locus of a constraint are defined the same way: constraints propagate along those reachable surfaces as held invariant in a frame moving with the mechanism.

In that locus, now a two dimensional set, constraints are represented for all possible configurations of the mechanism. A solution to the problem is still a curve or surface that crosses all loci consistently. However, the challenge and the opportunity is that now inconsistent constraints are not necessarily an issue, since we might have the freedom to chose a motion plan to avoid them, for example when designing the shape of a foot and the gate followed by the leg driving it.

9.2 Limitations and Future Directions

This thesis begins from the premise that we can represent mechanical function by providing a set of contacts. Although common in manipulation this might not always be sufficient. The direction and location of the contact force is important, but being able to produce a given contact normal, does not mean the effector will be able to exert enough force.

Friction is also critical to fully understand the reaction to contact. We could consider replacing the imposed contact normals by friction cones, to find shape solutions that satisfy the desired functionality but within the bounding conditions that yield stick/slip as desired.

There are also manipulation tasks, specially those involving large motions, which are not easily specified in terms of contacts. A more complete approach to design for the purpose of manipulation would need to reason within a common formulation both about contact and motion constraints.

For simplicity of exposition, when talking about contacts, we have referred only to matching the tangets of object and effector. However, to guarantee a compatible interaction, we might also want to constraint their relative curvatures. We can either approximate higher order constraints by a combination of first order ones, or directly impose a curvature constraint in a very similar fashion to tangential constraints: $(p, \kappa) \in \mathbb{R}^2 \times \mathbb{R}$ is satisfied by an effector $E(s,t)$ if there are $t_0 \in T$ and $s_0 \in S$ (or $(u_0, v_0) \in S$) such that:

$$E(s_0, t_0) = p \quad \text{and} \quad \left.\frac{\partial^2 E(s, t_0)}{\partial s^2}\right|_{s=s_0} = \kappa$$

The curvature is defined in the local coordinates of a curve, hence it is invariant to constraint propagation. If a problem is specified both in terms of tangential and curvature constraints, the loci will contain them both, and both should be considered in the integration step.

Finally, it is important to note that matching the tangent and curvature of object and effector might not even guarantee proper interaction. Both are local conditions that ensure that locally both surfaces will be compatible. However other sections of the effector or object might produce collision before reaching the imposed contact, as would often happen in concavities.

In general, guaranteeing global compatibility between object and effector is a very challenging problem that require global information for collision checking, that would prevent the closed form solutions obtained in this thesis. A more suitable strategy would be to turn the problem into an optimization formulation, and include in the optimization process other mechanical attributes, such as the parameters of the driving mechanism (location of rotation center or link lengths of linkage) and the freedom, if any in the description of the problem (location and direction of the desired contacts).

References

[1] Barrett. Barret Technologies: The Barret hand, 2001. URL http://www.barrett.com/robot/products-hand.htm.

[2] R.-P. Berretty, K. Y. Goldberg, M. H. Overmars, and A. F. van der Stappen. On Fence Design and the Complexity of Push Plans for Orienting Parts. In *Symposium on Computational Geometry (SCG)*, pages 21–29, 1997. ISBN 0897918789.

[3] R. P. Berretty, K. Y. Goldberg, M. H. Overmars, and A. F. van der Stappen. Trap Design for Vibratory Bowl Feeders. *The International Journal of Robotics Research*, 20(11):891–908, 2001.

[4] A. Bicchi, J. K. Salisbury, and D. L. Brock. Contact Sensing from Force Measurements. *The International Journal of Robotics Research*, 12(3):249–262, 1993.

[5] L. Birglen, C. Gosselin, and T. Laliberte. *Underactuated Robotic Hands*. Springer, 2008.

[6] G. Boothroyd and P. Dewhurst. *Design for Assembly: A Designer's Handbook*. Department of Mechanical Engineering, University of Massachusetts, Amherst, 1983.

[7] G. Boothroyd, C. Poli, and L. E. Murch. *Handbook of Feeding and Orienting Techniques for Small Parts*. Dept. of Mechanical Engineering at University of Massachussets, Amherst, 1977.

[8] D. L. Brock. Enhancing the Dexterity of a Robot Hand Using Controlled Slip. In *IEEE International Conference on Robotics and Automation (ICRA)*, pages 249–251, 1988.

[9] M. Brokowski, M. Peshkin, and K. Y. Goldberg. Optimal Curved Fences for Part Alignment on a Belt. *Journal of Mechanical Design*, 117(1):27–35, 1995.

[10] C. Cai and B. Roth. On the Spatial Motion of Rigid Bodies with Point Contact. In *IEEE International Conference on Robotics and Automation (ICRA)*, pages 686–695, 1987.

[11] M. E. Caine. *The Design of Shape from Motion Constraints*. PhD thesis, Massachusetts Institute of Technology, 1993.

[12] M. E. Caine. The Design of Shape Interactions Using Motion Constraints. In *IEEE International Conference on Robotics and Automation (ICRA)*, pages 366–371, 1994.

[13] J. F. Canny and K. Y. Goldberg. RISC for Industrial Robotics: Recent Results and Open Problems. In *IEEE International Conference on Robotics and Automation (ICRA)*, pages 1951–1958, 1994.

[14] M. Ciocarlie, F. M. Hicks, and S. Stanford. Kinetic and Dimensional Optimization for a Tendon-driven Gripper. In *IEEE International Conference on Robotics and Automation (ICRA)*, 2013.

[15] S. Collins, A. Ruina, R. Tedrake, and M. Wisse. Efficient Bipedal Robots Based on Passive-Dynamic Walkers. *Science*, 307(5712):1082–1085, 2005.

[16] M. R. Cutkosky. On Grasp Choice, Grasp Models, and the Design of Hands for Manufacturing Tasks. *IEEE Transactions on Robotics and Automation*, 5(3):269–279, June 1989. ISSN 1042296X.

[17] L. Decker, C. Berge, S. Renous, and X. Penin. An Alternative Approach to Normalization and Evaluation for Gait Patterns: Procrustes Analysis Applied to the Cyclograms of Sprinters and middle-Distance runners. *Journal of Biomechanics*, 40(9):2078–87, Jan. 2007.

[18] A. M. Dollar and R. D. Howe. Towards Grasping in Unstructured Environments: Grasper Compliance and Configuration Optimization. *Advanced Robotics*, 19(5):523–543, 2005.

[19] A. M. Dollar and R. D. Howe. Joint Coupling Design of Underactuated Grippers. In *Mechanisms and Robotics Conference (MR)*, pages 903–911, 2006.

[20] A. M. Dollar and R. D. Howe. The Highly Adaptive SDM Hand: Design and Performance Evaluation. *The International Journal of Robotics Research*, 29(5):585–597, Feb. 2010. ISSN 0278-3649.

[21] B. Faltings. Qualitative Kinematics in Mechanisms. *Artificial Intelligence*, 44(1-2):89–119, 1990.

[22] K. D. Forbus, P. Nielsen, and B. Faltings. Qualitative Spatial Reasoning: The CLOCK Project. *Artificial Intelligence*, 51(1-3):417–471, 1991.

[23] K. Y. Goldberg and H. Moradi. Compiling Assembly Plans into Hard Automation. In *IEEE International Conference on Robotics and Automation (ICRA)*, pages 1858–1863, 1996.

[24] M. Gomes and A. Ruina. Walking Model With no Energy Cost. *Physical Review E*, 83(3):6–9, 2011.

[25] C. M. Gosselin. Adaptive Robotic Mechanical Systems: A Design Paradigm. *Journal of Mechanical Design*, 128(1):192–198, 2006.

[26] R. Gupta and M. J. Jakiela. Simulation and Shape Synthesis of Kinematic Pairs via Small-Scale Interference Detection. *Research in Engineering Design*, 6(2):103–123, 1994.

[27] H. Hanafusa and H. Asada. Stable Prehension by a Robot Hand with Elastic Fingers. In *International Symposium of Industrial Robotics (ISIR)*, pages 361–368, 1977.

[28] R. S. Hartenberg and J. Denavit. *Kinematic Synthesys of Linakges*. McGraw-Hill, 1964.

[29] S. Hirose and Y. Umetani. Soft Gripper. In *International Symposium on Industrial Robots (ISIR)*, pages 112–127, 1983.

[30] J. M. Hollerback. Grasping in Human and Robot Hands. In *Vision and Action: The Control of Grasping*, pages 243–274. Ablex Pub, 1990.

[31] R. Jardine. Climbing Aids - US Patent 4184657, 1980.

[32] L. Joskowicz. *Reasoning about Shape and Kinematic Function in Mechanical Devices*. PhD thesis, New York University, 1988.

[33] L. Joskowicz and S. Addanki. From Kinematics to Shape: An Approach to Innovative Design. In *National Conference on Artificial Intelligence (NCAI)*, pages 347–352, 1988.

[34] G. A. Kragten, M. Baril, C. M. Gosselin, and J. L. Herder. Stable Precision Grasps by Underactuated Grippers. *IEEE Transactions on Robotics*, 27(6):1056–1066, 2011.

[35] T. Laliberte and C. M. Gosselin. Actuation System for Highly Underatuated Gripping Mechanism - US Patent 6505870, 2003.

[36] T. Lozano-Perez. Spatial Planning: A Configuration Space Approach. *IEEE Transactions on Computers*, C-32(2):108–120, Feb. 1983.

[37] T. Lozano-Perez. Motion Planning and the Design of Orienting Devices for Vibratory Part Feeders. Technical report, Artificial Intelligence Laboratory, Massachusetts Institute of Technology, 1986.

[38] E. Lucas. Huitieme Recreation-La Machine a Marcher. *Recreat. Math*, 4:198–204, 1894.

[39] K. M. Lynch, N. Shiroma, H. Arai, and K. Tanie. The Roles of Shape and Motion in Dynamic Manipulation: The Butterfly Example. In *IEEE International Conference on Robotics and Automation (ICRA)*, pages 1958–1963. Ieee, 1998. ISBN 0-7803-4300-X.

[40] M. T. Mason, S. S. Srinivasa, and A. S. Vazquez. Generality and Simple Hands. In *International Symposium on Robotics Research (ISRR)*, 2009.

[41] M. T. Mason, A. Rodriguez, S. S. Srinivasa, and A. S. Vazquez. Autonomous Manipulation with a General-Purpose Simple Hand. *The International Journal of Robotics Research*, 31(5):688–703, 2012.

[42] M. McCarthy. *Introduction to Theoretical Kinematics*. The MIT Press, 1990.

[43] T. McGeer. Passive Dynamic Walking. *The International Journal of Robotics Research*, 9(2): 62–82, 1990.

[44] D. J. Montana. The Kinematics of Contact and Grasp. *The International Journal of Robotics Research*, 7(3):17–32, 1988.

[45] E. Z. Moore, D. Campbell, F. Grimminger, and M. Buehler. Reliable Stair Climbing in the Simple Hexapod "RHex". In *IEEE International Conference on Robotics and Automation (ICRA)*, pages 2222–2227, 2002.

[46] J. Napier and R. H. Tuttle. *Hands*. Princeton University Press, 1993.

[47] L. Odhner, L. P. Jentoft, M. R. Claffee, N. Corson, Y. Tenzer, M. Raymond R, M. Buehler, R. Kohout, R. D. Howe, and A. M. Dollar. A Compliant, Underactuated Hand for Robust Manipulation. *Computer Research Repository (CoRR) - arXiv*, 2013. URL http://arxiv.org/abs/1301.4394.

[48] T. Okada. Object-Handling System for Manual Industry. *IEEE Transactions on Systems, Man, and Cybernetics*, 9(2):79–89, 1979.

[49] R. Paolini, A. Rodriguez, S. S. Srinivasa, and M. T. Mason. A Data-Driven Statistical Framework for Post-Grasp Manipulation. In *International Symposium on Experimental Robotics (ISER)*, 2012.

[50] R. Paolini, A. Rodriguez, S. S. Srinivasa, and M. T. Mason. A Data-Driven Statistical Framework for Post-Grasp Manipulation. *The International Journal of Robotics Research - Conditionally Accepted*, 2013.

[51] B. Paul. *Kinematics and Dynamics of Planar Machinery*. Prentice-Hall, 1979.

[52] M. Peshkin and A. Sanderson. Planning Robotic Manipulation Strategies for Workpieces that Slide. *IEEE Journal on Robotics and Automation*, 4(5):524–531, 1988.

[53] R. Pfeifer and F. Iida. Morphological Computation: Connecting Body, Brain and Environment. *Japanese Scientific Monthly*, 58(2):48–54, 2005.

[54] M. H. Raibert. *Legged Robots That Balance*. The MIT Press, 1986.

[55] A. H. Redford and G. Boothroyd. Vibratory Feeding. *Proceedings of the Institution of Mechanical Engineers*, 182(6):135–152, 1967.

[56] A. H. Redford, E. K. Lo, and P. J. Killeen. Parts Feeder for a Multi-Arm Assembly Robot. In *15th CIRP Seminar on Manufacturing Systems*, 1983.

[57] F. Reuleaux. *The Kinematics of Machinery: Outlines of a Theory of Machines*. Macmillan, 1876.

[58] RobotIQ. Robotiq Adaptive Gripper: Specification Sheet, 2010. URL http://www.robotiq.com.

[59] A. Rodriguez and M. T. Mason. Grasp Invariance. In *Algorithmic Foundations of Robotics (WAFR)*, 2010.

[60] A. Rodriguez and M. T. Mason. Grasp Invariance. *The International Journal of Robotics Research*, 31(2):237–249, 2012.

[61] A. Rodriguez and M. T. Mason. Effector Form Design for 1DOF Planar Actuation. In *IEEE International Conference on Robotics and Automation (ICRA)*, 2013.

[62] A. Rodriguez, M. T. Mason, and S. S. Srinivasa. Manipulation Capabilities with Simple Hands. In *International Symposium on Experimental Robotics (ISER)*, 2010.

[63] A. Rodriguez, M. T. Mason, S. S. Srinivasa, M. Bernstein, and A. Zirbel. Abort and Retry in Grasping. In *IEEE International Conference on Intelligent Robots and Systems (IROS)*, 2011.

[64] B. Rubinger, P. Fulford, L. Gregoris, C. M. Gosselin, and T. Laliberte. Self-Adapting Robotic Auxiliary Hand (SARAH) for SPDM Operations on the International Space Station. In *International Symposium on Artificial Intelligence and Robotics and Automation in Space (i-SAIRAS)*, 2001.

[65] J. K. Salisbury and J. J. Craig. Articulated Hands: Force Control and Kinematic Issues. *The International Journal of Robotics Research*, 1(1):4–17, 1982.

[66] U. Saranli, M. Buehler, and D. E. Koditschek. RHex: A Simple and Highly Mobile Hexapod Robot. *The International Journal of Robotics Research*, 20(7):616–631, 2001.

[67] G. Schlesinger. *Der Mechanische Aufbau der Kunstlichen Glieder. Ersatzglieder und Arbeitshilfen, part II.* Springer, 1919.

[68] J. E. Shigley and J. J. Uicker. *Theory of Machines and Mechanisms.* McGraw-Hill, 1980.

[69] A. Svoboda. *Computing Mechanisms and Linkages.* McGraw-Hill, 1948.

[70] D. A. Theobald, W. J. Hong, A. Madhani, B. Hoffman, G. Niemeyer, L. Cadapan, J. J. Slotine, and J. K. Salisbury. Autonomous Rock Acquisition. In *AIAA Forum on Advanced Developments in Space Robotics*, 1996.

[71] D. W. Thompson. *On Growth and Form.* Cambridge University Press, 1961.

[72] J. A. Thorpe. *Elementary Topics in Differential Geometry.* Springer, 1979.

[73] J. Trinkle and R. Paul. Planning for Dexterous Manipulation with Sliding Contacts. *The International Journal of Robotics Research*, 9(3):24–48, 1990.

[74] N. T. Ulrich. *Grasping with Mechanical Intelligence.* Master thesis, University of Pennsylvania, 1989.

[75] N. T. Ulrich, R. Paul, and R. Bajcsy. A Medium-Complexity Compliant End Effector. In *IEEE International Conference on Robotics and Automation (ICRA)*, pages 434–436, 1988.

[76] D. E. Whitney, R. E. Gustavson, and M. P. Hennessey. Designing Chamfers. *The International Journal of Robotics Research*, 2(4):3–18, 1983.

[77] J. Wiegley, K. Y. Goldberg, M. Peshkin, and M. Brokowski. A Complete Algorithm for Designing Passive Fences to Orient Parts. *Assembly Automation*, 17(2):129–136, 1997.

[78] M. T. Zhang and K. Y. Goldberg. Gripper Point Contacts for Part Alignment. *IEEE Transactions on Robotics and Automation*, 18(6):902–910, 2002.